Table 4
DNA and RNA regulatory transcripts

Probe set	Day 1 in vivo		Day 29 in vivo		Annotation of gene represented by probe set
	Fold difference	SAM q value	Fold difference	SAM q value	
149.m00092_at	6.88	0.01	2.78	0.18	Hypothetical protein 149.t00006
169.m00139_at	4.56	0.01	1.98	0.41	Hypothetical protein 169.t00027
55.m00187_at	3.89	0.01	2.46	0.25	Hypothetical protein 55.t00025
146.m00110_at	2.87	0.04	1.25	0.7	Myb family DNA-binding protein
123.m00114_at	2.54	0	−1.55	0.28	Hypothetical protein 123.t00010
94.m00147_at	2.53	0.03	3.35	0.14	Hypothetical protein 94.t00018
20.m00305_at	2.44	0.49	4.05	0.02	RNA-binding protein, putative
197.m00084_x_at[a]	2.35	0.03	1.29	0.64	Hypothetical protein 197.t00015
524.m00023_at	2.3	0.01	1.38	0.69	Myb family DNA-binding protein
20.m00272_at	2.23	0.06	−6.25	0	Conserved hypothetical protein (DNA binding group)
3.m00577_at	2	0.01	6.55	0.09	High mobility group protein, putative
275.m00123_s_at[b]	1.92	0.04	2.34	0.38	Protein kinase, putative
98.m00143_at	1.86	0.05	−1.37	0.45	Zinc finger protein, putative
5.m00408_s_at[c]	1.82	0.25	−1.43	0.5	Hypothetical protein 5.t00017
4.m00655_at	1.75	0.19	7.36	0	Hypothetical protein 4.t00077
143.m00093_at	−1	0.42	−5.81	0.01	Conserved hypothetical protein (DNA binding group)
227.m00086_at	−1.09	0.42	−16.64	0	Conserved hypothetical protein (DNA binding group)
177.m00126_s_at[d]	−1.16	0.36	−4.09	0.04	Ribonuclease, putative
198.m00105_at	−1.26	0.16	−2.13	0.02	RNA-binding protein, putative
173.m00119_at	−1.37	0.12	−2.62	0.04	Putative CLK family kinase (*Dictyostelium discoideum*)
324.m00040_at[e]	−1.51	0.16	−4.21	0	Transcription initiation factor TFIID, putative
111.m00140_x_at[a]	−1.92	0.04	−11.04	0	Conserved hypothetical protein (DNA binding group)
62.m00167_at	−2.01	0.02	−1.4	0.28	Hypothetical protein 62.t00018
147.m00097_x_at[a,f]	−2.03	0.02	1.17	0.7	Enhancer binding protein-1
490.m00035_at	−2.07	0.03	−1.64	0.32	Hypothetical protein 490.t00001
268.m00065_x_at[a]	−2.19	0.01	−1.12	0.6	Predicted: similar to myb binding protein (P160) 1a-like (*Strongylocentrotus purpuratus*)
91.m00190_s_at[g]	−2.29	0.05	−2.48	0	RNA-binding protein, putative
88.m00155_s_at	−2.47	0.02	−2.08	0.11	Hypothetical protein 88.t00011
38.m00215_at	−2.53	0.04	−1.44	0.41	AAA family ATPase
14.m00334_at	−4.68	0.03	−1.47	0.41	Hypothetical protein 14.t00055

[a] (_at) probe sets represent single genes, s_at. probe sets recognize two or more genes with which the probes are an exact match, _x_at probe sets may cross-hybridize in an unpredictable manner with sequences other than the main target.
[b] 275.m00123 also represents 275.m00093 a truncated version that also contains an internal deletion of 24 nts.
[c] 5.m00408_s also represents 183.m00107 with which it is completely identical.
[d] 177.m00126_s_at also represents 100.m00129 with which it is 98% identical.
[e] This gene has been previously described by Luna-Arias et al. [42].
[f] Regulator of the transcription of the *hgl5* large subunit of the Gal/GalNAc lectin, Schaenman et al. [31].
[g] 91.m00190_s represents also the 204.m00092 ORF to which it is completely identical.

Vam3 homologue and a Ras-related gene (128.m00135) were down-regulated in vivo, while the transcripts of three Ras-related proteins (Ras-related protein 3, and two Rab family GTPases) and a Syntaxin C (yeast Pep13 homologue) (167.m00134) were increased at Day 1 (Table 5 and supplemental data). Although the Rab family GTPases mRNA levels remained high at Day 29 they were not statistically different from in vitro levels. Other genes, including those encoding potential Rho and Ras GTPase activating proteins, were down-regulated, and as previously mentioned, the phosphoinositide 3-kinase transcript was statistically decreased (Table 5 and supplemental data). These data suggest that the parasite alters the regulation of cytoskeletal-mediated processes in response to the host environment.

3.13. Unknown proteins

An intriguing result was the modulation of expression of four groups of hypothetical proteins (Table 6). Group 1 genes were similar to the AIG proteins implicated in plant defense from bacteria [38]. The group 1 transcripts were either un-regulated or up-regulated at Day 1, and with only two exceptions (AIG40.m00239 and AIG451.m00039) they were decreased at Day 29. Group 2 genes contained bacterial surface protein A-like sequences (BspA). Three members of the *E. histolytica* BspA family were modulated in vivo (BspA32 transcript was repressed at Days 1 and 29, BspA615.m00022 was decreased two-fold at Day 1, and BspA707.m00012 gene was up-regulated at Day 29) [33,39]. Group 3 genes encode small (~4–8 kDa) basic and

Table 5
Changes in transcripts potentially involved in intracellular signaling

Probe set	Day 1 in vivo		Day 29 in vivo		Annotation of gene represented by probe set
	Fold difference	SAM q value	Fold difference	SAM q value	
Transmembrane kinases					
A subgroup					
148.m00080_at[a]	4.66	0	2.31	0.5	TMK69
16.m00305_x_at[a,b]	3.01	0.01	1.47	0.68	TMK53
2.m00624_s_at	2.38	0.01	2.56	0.01	Protein kinase, putative
152.m00104_at[a]	−2	0.05	−3	0.02	TMK17
B1 subgroup					
67.m00091_x_at[a,b]	3.89	0.01	2.1	0.53	TMK95
174.m00087_x_at[b]	2.74	0.02	1.84	0.6	Protein kinase, putative
New subgroup					
251.m00091_at	−1.6	0.07	−2.67	0	Receptor protein kinase, putative
B2 subgroup					
15.m00355_at[a]	3.11	0.01	1.46	0.64	TMK105
C subgroup					
20.m00345_at[a]	2.81	0.02	1.67	0.5	TMK63
D1 subgroup					
5.m00482_at[a]	2.61	0.02	1.7	0.67	TMK56
136.m00104_at[a]	−2.76	0	−4.76	0	TMK03
Other kinases					
406.m00055_s_at[c]	2.02	0.03	2.77	0.25	Protein kinase
265.m00084_s_at[d]	1.45	0.51	−2.47	0	Protein kinase
16.m00336_s_at[e]	1.03	0.42	−2.03	0.04	Protein kinase
1.m00709_at	−1.01	0.42	−3.27	0.01	Polynucleotide kinase-3-phosphatase
9.m00406_s_at[f]	−1.08	0.36	−2.25	0	Phosphatidylinositol 3-kinase
77.m00170_at	−1.87	0.01	−2.35	0.02	Protein kinase
8.m00424_at	−2.16	0.04	−3.02	0	Protein kinase
116.m00121_at	−2.47	0.01	−11.01	0	Protein kinase
34.m00274_at	−3.48	0.02	−1.84	0.12	Protein kinase
Phosphatases					
98.m00146_at	2.08	0.04	−1.12	0.57	Ser/Thr protein phosphatase family protein (*Colwellia psychrerythraea* 34H)
92.m00163_x_at[b]	2.01	0.05	1.57	0.47	Conserved hypothetical protein
8.m00389_at	−1.08	0.42	−2.15	0.04	Protein phosphatase
58.m00145_at	−2	0.05	−1.03	0.65	Protein tyrosine phosphatase
171.m00101_at	−2.01	0.03	−1.22	0.53	Amidohydrolase
107.m00111 at	−2.09	0.05	−1.38	0.47	Protein phosphatase
393.m00036_at	−2.12	0.04	−1.24	0.47	Ser Thr protein phosphatase
69.m00153_at	−2.35	0.02	−2.37	0.04	Ser Thr protein phosphatase
289.m00068_at	−2.66	0.02	−2.83	0.05	Amidohydrolase
16.m00311_at	−3.19	0.02	−2.19	0.09	Hypothetical protein
Calcium binding					
3.m00563_at[g]	5.65	0	2.9	0.35	Calcium-binding protein Calcium Binding family
56.m00149_at[h]	4.31	0	4.33	0	Calcium-binding protein
94.m00131_at	4.12	0.01	1.27	0.64	SPRY domain protein
15.m00302_at	2.99	0.05	2.03	0.16	Hypothetical protein 15.t00011
247.m00081_s_at[i]	−2.03	0.01	−1.64	0.09	Grainin 2
32.m00201_s_a[i]	−2.12	0.01	−1.19	0.53	Conserved hypothetical protein
182.m00137_at[k]	−2.21	0.03	−2.73	0.08	Grainin 1
195.m00083_s_at[l]	−2.29	0.04	1.47	0.7	Plasma membrane calcium-transporting ATPase
101.m00121_at[g]	−2.51	0.01	−2.1	0.22	C2 domain protein Calcium Binding family
Small GTPase					
110.m00125_at	5.71	0	N/A	N/A	Hypothetical protein 110.t00013/GTPase-activator protein for Ras-like GTPase
288.m00067_at[m]	4.73	0	4.25	0.53	Ras-related protein 3
30.m00275_at	4.32	0.01	2.25	0.11	Rab family GTPase

Table 5 (*Continued*)

Probe set	Day 1 in vivo		Day 29 in vivo		Annotation of gene represented by probe set
	Fold difference	SAM q value	Fold difference	SAM q value	
71.m00153_at	3.32	0.03	3.23	0.08	Rho family GTPase
8.m00373_at	3.18	0	1.05	0.7	Ras guanine nucleotide exchange factor
106.m00140_at	3.04	0.03	1.49	0.6	Rap/Ran GTPase activating protein
4.m00593_at	2.95	0	2.86	0.28	Rab family GTPase
233.m00108_at	1.05	0.51	2.64	0.05	Alanine aminotransferase, RanBP1 domain
6.m00423_x_at[b]	−1.52	0.07	−4.16	0	Hypothetical protein 6.t00021 GTPase-activator protein for Ras-like GTPase
60.m00155_at	−1.61	0.04	−2.26	0	Hypothetical protein 60.t00020 GTPase-activator protein for Ras-like GTPase
47.m00168_x_at[b]	−1.7	0.07	−2.07	0.02	Ran-binding protein
24.m00315_s_at[n]	−2.07	0.01	−1.59	0.22	Rho GTPase activating protein
128.m00135_at	−2.16	0.03	−1.67	0.16	Ras family GTPase
265.m00063_x_at[b]	−2.24	0.01	−1.62	0.22	Rho guanine nucleotide exchange factor
1.m00710_at	−2.28	0.05	−2.82	0.02	Rho GTPase activating protein
334.m00040_at	−2.29	0.03	−1.26	0.53	Ras guanine nucleotide exchange factor
3.m00556_at	−2.42	0.02	−2.69	0.06	Hypothetical protein 3.t00019 small GTPase mediated signal transduction
131.m00145_at	−2.43	0.01	−1.83	0.05	Ras guanine nucleotide exchange factor
4.m00698_at	−2.57	0.03	−1.55	0.38	Rap/Ran GTPase activating protein
157.m00102_at	−3.2	0.01	−3.86	0	Rho GTPase activating protein
10.m00354_at	−5.05	0.01	−2	0.05	Hypothetical protein 10.t00038 GTPase-activator protein for Ras-like GTPase
151.m00103_at	−6.47	0	−4.41	0.01	Rho guanine nucleotide exchange factor

[a] Gene family previously described by Beck et al. [33].

[b] (_at) probe sets represent single genes, s_at. probe sets recognize two or more genes with which the probes are an exact match, _x_at probe sets may cross-hybridize in an unpredictable manner with sequences other than the main target.

[c] 406.m00055_s_at also represents 169.m00134 with which it is identical.

[d] 265.m00084_s at also represents 265.m00081with which it is identical.

[e] 16.m00336_s_at also represents 72.m00163 as they have an identical internal stretch of 808 nts.

[f] 9.m00406_s_at also represents 67.m00102 with which it is 82% identical.

[g] H. Moreno, personal communication.

[h] EhCaBP has been previously described by Sahoo et al. [36].

[i] 247.m00081_s_at is truncated by 69 nts but otherwise identical to 224.m00108 and 224.m00112 which are identical to each other. This gene has been previously described as grainin 2 by Nickel et al. [37].

[j] 32.m00210 represents 364.m00044 of which it is a truncated (575) 99% identical version.

[k] 182.m00137 was over 85% similar to grainin 1 which was previously described by Nickel et al. [37].

[l] 195.m00083_s_at represents 429.m00044 with which it is identical.

[m] 288.m00067 has been previously described as the Ras-related protein 3 by Kumagai et al. [43].

[n] 24.m00315_s also represents 13.m00346, these ORF's were identical but for an internal deletion of 60 nts.

cysteine rich proteins, which are over 97% identical at the protein level. These were significantly repressed at Day 29. Group 4 genes had some similarity to the TLDc domain of LysM, a protein with peptidoglycan-binding bacteriolytic and adhesive activities. Only two transcripts of the Group 4 TLDc gene family were expressed sufficiently highly to be included in our present analysis, with transcripts at Day 29 significantly increased when contrasted with the Day 1 in vivo levels.

3.14. Summary

This study is the first genome-wide analysis of transcription in *E. histolytica* trophozoites, and the first description of gene expression in trophozoites from the intestine. The most important findings were that >80% of ORFs are transcribed in trophozoites, and that in response to the host intestinal environment alterations occurred in the expression of genes implicated in metabolism, oxygen defense, cell signaling, virulence, antibacterial activity, and DNA-binding.

The inconsistent changes in the laterally-transferred metabolic enzymes suggest that the derivation of these genes did not lead to common regulation in response to the intestinal environment. Interestingly several members of the large gene families of *E. histolytica* were also regulated differently (e.g. the cysteine protease family Table 2) which suggested that, despite their similarity, the encoded proteins have distinct functions important in the adaptation of *E. histolytica* to the host environment.

It should be noted that there are several limitations to the approaches used in this report. Most importantly, changes in the level of mRNA abundance are only one level of control of gene expression. Ultimately the understanding of the parasite adaptation to the host will require deciphering the not

Table 6
Subgroups of unknown genes significantly changed between Days 1 and 29

Probe set	Day one in vivo		Day 29 in vivo		Annotation of gene represented by probe set
	Fold difference	SAM q value	Fold difference	SAM q value	
Group 1					
374.m00023_at	4.52	0.01	−1.84	0.2	AIG1 family protein, putative
451.m00039_at	3.62	0.05	3	0.53	AIG1 family protein, putative
374.m00021_at	2.79	0.01	−1.68	0.25	AIG1 family protein, putative
499.m00017_x_at[a]	2.43	0.02	−1.4	0.32	AIG1 family protein, putative
499.m00016_x_at[a]	2.1	0.03	−2.46	0.2	AIG1 family protein, putative
432.m00030_at	1.67	0.39	−34.8	0	AIG1 family protein, putative
432.m00029_at	1.6	0.16	−11.27	0	AIG1 family protein, putative
40.m00239_at	1.47	0.45	5.08	0.04	AIG1 family protein, putative
628.m00011_at	1.28	0.42	−3.15	0	AIG1 family protein, putative
477.m00021_at	1.08	0.42	−5.72	0.01	AIG1 family protein, putative
374.m00024_x_at[a]	1.07	0.51	−4.1	0	AIG1 family protein, putative
71.m00149_at	−1.86	0.09	−24.56	0	AIG1 family protein, putative
BspA-like[b]					
707.m00012_x_at[a]	2.08	0.16	7.08	0	BspA-like leucine rich repeat protein, putative
615.m00022_x_at[a]	−2.76	0.05	1.21	0.7	BspA-like leucine rich repeat protein, putative
7.m00417_a[c]	−2.84	0.02	−4.08	0.01	BspA-like leucine rich repeat protein, BspA32
Group 3					
496.m00027_x_at[a]	2.59	0.06	−3.72	0	Hypothetical protein 496.t00004
493.m00030_x_at[a]	2.57	0.12	−3.93	0	Hypothetical protein 493.t00001
586.m00015_s_at[d]	2.19	0.25	−4.06	0	Hypothetical protein
Group 4					
65.m00145_x_at[a]	2.25	0.02	14.75	0	Hypothetical protein 65.t00007
395.m00029_x_at[a]	−1.05	0.51	3.15	0.28	Conserved hypothetical protein

[a] (_at) probe sets represent single genes, s_at probe sets recognize two or more genes with which the probes are an exact match, _x_at probe sets may cross-hybridize in an unpredictable manner with sequences other than the main target.
[b] Gene family previously described by Davis et al. [39].
[c] Previously described by Beck et al. [33].
[d] 586.m00015_s represents also the 496.m00027 ORF which differs by two nucleotides.

only the transcriptome, but also the *E. histolytica* proteome and metabolome. The analysis of the transcriptome is in turn limited by the fact that it was not possible to independently represent every ORF on the array, because of the presence of families of genes with high sequence identity. In addition, the gene array hybridizations necessitated amplification of the amebic RNA, a step that introduces potential artifacts from non-linear amplification. However, the amplification used a technique that limits non-linear amplification. In addition, the array data was independently verified for 11/12 genes by quantitative real-time reverse transcriptase PCR from unamplified mRNA, suggesting that unequal amplification of mRNA was not a systematic problem with this analysis.

The description of the trophozoite transcriptome establishes the foundation for future interventional studies to delineate the contributions of the altered gene products to intestinal colonization and invasion. The long-term outcome of these studies promises to provide a molecular understanding of the parasite factors controlling the formation of amebic colitis, the most common and feared manifestation of amebiasis.

Acknowledgments

This work was supported by NIH Grant AI 39741 and Biotechnology Engagement Program Grant 17. The bioinformatics data analysis at VBI was funded by Department of Defense grant #DAAD 13-02-C-0018. We thank Dr P. Hoffman for advice and helpful discussion.

Appendix A. Supplementary data

Supplementary data associated with this article can be found, in the online version, at doi:10.1016/j.molbiopara.2006.02.007.

References

[1] Clark CG, Roger AJ. Direct evidence for secondary loss of mitochondria in *Entamoeba histolytica*. Proc Natl Acad Sci U S A 1995;92:6518–21.
[2] Field J, Rosenthal B, Samuelson J. Early lateral transfer of genes encoding malic enzyme, acetyl-CoA synthetase and alcohol dehydrogenases from anaerobic prokaryotes to *Entamoeba histolytica*. Mol Microbiol 2000;38:446–55.
[3] Loftus B, Anderson I, Davies R, Alsmark UC, Samuelson J, et al. The genome of the protist parasite *Entamoeba histolytica*. Nature 2005;433:865–8.
[4] Stanley Jr SL. Amoebiasis. Lancet 2003;361:1025–34.
[5] Petri Jr WA, Haque R, Mann BJ. The bittersweet interface of parasite and host: lectin-carbohydrate interactions during human invasion by the parasite *Entamoeba histolytica*. Annu Rev Microbiol 2002;56:39–64.
[6] Diamond LS, Harlow DR, Cunnick C. A new medium for axenic cultivation of *Entamoeba histolytica* and other Entamoeba. Trans R Soc Trop Med Hyg 1978;72:431–2.

[7] Houpt ER, Glembocki DJ, Obrig TG, Moskaluk CA, Lockhart LA, et al. The mouse model of amebic colitis reveals mouse strain susceptibility to infection and exacerbation of disease by CD4+ T cells. J Immunol 2002;169:4496–503.

[8] Brazma A, Hingamp P, Quackenbush J, Sherlock G, Spellman P, et al. Minimum information about a microarray experiment (MIAME)-toward standards for microarray data. Nat Genet 2001;29:365–71.

[9] Wu Z, Irizarry R, Gentleman R, Murillo F, Spencer F. A model based background adjustment for oligonucleotide expression arrays. Technical report, 2003, John Hopkins University, Department of Biostatistics Working Papers, Baltimore, MD, 2004.

[10] Ginzinger DG. Gene quantification using real-time quantitative PCR: an emerging technology hits the mainstream. Exp Hematol 2002;30:503–12.

[11] Vandesompele J, De Preter K, Pattyn F, Poppe B, Van Roy N, et al. Accurate normalization of real-time quantitative RT-PCR data by geometric averaging of multiple internal control genes. Genome Biol 2002;3 [RESEARCH0034].

[12] Bruchhaus I, Loftus BJ, Hall N, Tannich E. The intestinal protozoan parasite *Entamoeba histolytica* contains 20 cysteine protease genes, of which only a small subset is expressed during in vitro cultivation. Eukaryot Cell 2003;2:501–9.

[13] Tokoro M, Asai T, Kobayashi S, Takeuchi T, Nozaki T. Identification and characterization of two isoenzymes of methionine gamma-lyase from *Entamoeba histolytica*: a key enzyme of sulfur-amino acid degradation in an anaerobic parasitic protist that lacks forward and reverse transsulfuration pathways. J Biol Chem 2003;278:42717–27.

[14] Nozaki T, Ali V, Tokoro M. Sulfur-containing amino acid metabolism in parasitic protozoa. In: Baker J, Muller R, Rollinson D, editors. Advances in Parasitology. Academic Press; 2005. p. 1–100.

[15] Nixon JE, Field J, McArthur AG, Sogin ML, Yarlett N, et al. Iron-dependent hydrogenases of *Entamoeba histolytica* and *Giardia lamblia*: activity of the recombinant entamoebic enzyme and evidence for lateral gene transfer. Biol Bull 2003;204:1–9.

[16] Rosenthal B, Mai Z, Caplivski D, Ghosh S, de la Vega H, et al. Evidence for the bacterial origin of genes encoding fermentation enzymes of the amitochondriate protozoan parasite *Entamoeba histolytica*. J Bacteriol 1997;179:3736–45.

[17] Bruchhaus I, Roeder T, Lotter H, Schwerdtfeger M, Tannich E. Differential gene expression in *Entamoeba histolytica* isolated from amoebic liver abscess. Mol Microbiol 2002;44:1063–72.

[18] Ali V, Shigeta Y, Tokumoto U, Takahashi Y, Nozaki T. An intestinal parasitic protist, *Entamoeba histolytica*, possesses a non-redundant nitrogen fixation-like system for iron–sulfur cluster assembly under anaerobic conditions. J Biol Chem 2004;279:16863–74.

[19] Filenko NA, Browning DF, Cole JA. Transcriptional regulation of a hybrid cluster (prismane) protein. Biochem Soc Trans 2005;33:195–7.

[20] van den Berg WA, Hagen WR, van Dongen WM. The hybrid-cluster protein ('prismane protein') from *Escherichia coli*. Characterization of the hybrid-cluster protein, redox properties of the [2Fe–2S] and [4Fe–2S–2O] clusters and identification of an associated NADH oxidoreductase containing FAD and [2Fe–2S]. Eur J Biochem 2000;267:666–76.

[21] Akbar MA, Chatterjee NS, Sen P, Debnath A, Pal A, et al. Genes induced by a high-oxygen environment in *Entamoeba histolytica*. Mol Biochem Parasitol 2004;133:187–96.

[22] Samarawickrema NA, Brown DM, Upcroft JA, Thammapalerd N, Upcroft P. Involvement of superoxide dismutase and pyruvate:ferredoxin oxidoreductase in mechanisms of metronidazole resistance in *Entamoeba histolytica*. J Antimicrob Chemother 1997;40:833–40.

[23] Tekwani BL, Mehlotra RK. Molecular basis of defence against oxidative stress in *Entamoeba histolytica* and *Giardia lamblia*. Microbes Infect 1999;1:385–94.

[24] Bruchhaus I, Tannich E. Induction of the iron-containing superoxide dismutase in *Entamoeba histolytica* by a superoxide anion-generating system or by iron chelation. Mol Biochem Parasitol 1994;67:281–8.

[25] Saavedra E, Encalada R, Pineda E, Jasso-Chavez R, Moreno-Sanchez R. Glycolysis in *Entamoeba histolytica*. Biochemical characterization of recombinant glycolytic enzymes and flux control analysis. FEBS J 2005;272:1767–83.

[26] Deng Z, Huang M, Singh K, Albach RA, Latshaw SP, et al. Cloning and expression of the gene for the active PPi-dependent phosphofructokinase of *Entamoeba histolytica*. Biochem J 1998;329:659–64.

[27] Chi AS, Deng Z, Albach RA, Kemp RG. The two phosphofructokinase gene products of *Entamoeba histolytica*. J Biol Chem 2001;276:19974–81.

[28] Wolfe AJ. The acetate switch. Microbiol Mol Biol Rev 2005;69:12–50.

[29] Zuo X, Coombs GH. Amino acid consumption by the parasitic, amoeboid protists *Entamoeba histolytica* and *E. invadens*. FEMS Microbiol Lett 1995;130:253–8.

[30] Anderson IJ, Loftus BJ. *Entamoeba histolytica*: observations on metabolism based on the genome sequence. Exp Parasitol 2005;110:173–7.

[31] Schaenman JM, Gilchrist CA, Mann BJ, Petri Jr WA. Identification of two *Entamoeba histolytica* sequence-specific URE4 enhancer-binding proteins with homology to the RNA-binding motif RRM. J Biol Chem 2001;276:1602–9.

[32] Sapra AK, Arava Y, Khandelia P, Vijayraghavan U. Genome-wide analysis of pre-mRNA splicing: intron features govern the requirement for the second-step factor, Prp17 in *Saccharomyces cerevisiae* and *Schizosaccharomyces pombe*. J Biol Chem 2004;279:52437–46.

[33] Beck DL, Boettner DR, Dragulev B, Ready K, Nozaki T, et al. Identification and gene expression analysis of a large family of transmembrane kinases related to the Gal/GalNAc lectin in *Entamoeba histolytica*. Eukaryot Cell 2005;4:722–32.

[34] Ghosh SK, Samuelson J. Involvement of p21racA, phosphoinositide 3-kinase, and vacuolar ATPase in phagocytosis of bacteria and erythrocytes by *Entamoeba histolytica*: suggestive evidence for coincidental evolution of amebic invasiveness. Infect Immun 1997;65:4243–9.

[35] Meza I, Clarke M. Dynamics of endocytic traffic of *Entamoeba histolytica* revealed by confocal microscopy and flow cytometry. Cell Motil Cytoskeleton 2004;59:215–26.

[36] Sahoo N, Labruyere E, Bhattacharya S, Sen P, Guillen N, et al. Calcium binding protein 1 of the protozoan parasite *Entamoeba histolytica* interacts with actin and is involved in cytoskeleton dynamics. J Cell Sci 2004;117:3625–34.

[37] Nickel R, Jacobs T, Urban B, Scholze H, Bruhn H, et al. Two novel calcium-binding proteins from cytoplasmic granules of the protozoan parasite *Entamoeba histolytica*. FEBS Lett 2000;486:112–6.

[38] Reuber TL, Ausubel FM. Isolation of Arabidopsis genes that differentiate between resistance responses mediated by the RPS2 and RPM1 disease resistance genes. Plant Cell 1996;8:241–9.

[39] Davis PH, Zhang Z, Chen M, Zhang X, Chakraborty S, et al. Identification of a family of BspA like surface proteins of *Entamoeba histolytica* with novel leucine rich repeats. Mol Biochem Parasitol 2005.

[40] Nozaki T, Asai T, Kobayashi S, Ikegami F, Noji M, et al. Molecular cloning and characterization of the genes encoding two isoforms of cysteine synthase in the enteric protozoan parasite *Entamoeba histolytica*. Mol Biochem Parasitol 1998;97:33–44.

[41] Garcia-Rivera G, et al. *Entamoeba histolytica*: a novel cysteine protease and an adhesin form the 112 kDa surface protein. Mol Microbiol 1999;33(3):556–68.

[42] Luna-Arias JP, et al. The TATA-box binding protein of *Entamoeba histolytica*: cloning of the gene and location of the protein by immunofluorescence and confocal microscopy. Microbiology 1999;145(Part 1):33–40.

[43] Kumagai M, et al. Molecular cloning and characterization of a protein farnesyltransferase from the enteric protozoan parasite *Entamoeba histolytica*. J Biol Chem 2004;279(3):2316–23.

Volume 55, Issue 4 December 2006 ISSN 1383-5769

PARASITOLOGY INTERNATIONAL

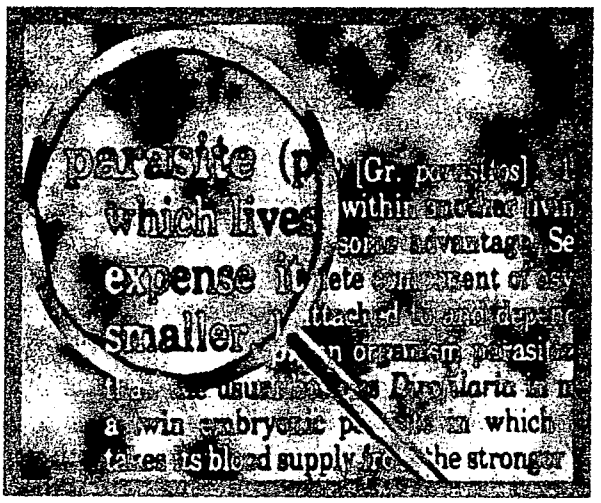

www.elsevier.com/locate/parint

Available online at www.sciencedirect.com
ScienceDirect
Parasitology International 55 (2006) 307–311
www.elsevier.com/locate/parint

Short communication

Genetic diversity of glucose phosphate isomerase from *Entamoeba histolytica*☆

Elham Razmjou [a], Ali Haghighi [b], Mostafa Rezaian [a], Seiki Kobayashi [c], Tomoyoshi Nozaki [d,*]

[a] *Department of Medical Parasitology and Mycology, School of Public Health and Institute of Public Health Research, Tehran University of Medical Sciences, Iran*
[b] *Department of Parasitology and Mycology, Shaheed Beheshti University of Medical Sciences, Iran*
[c] *Department of Tropical Medicine and Parasitology, School of Medicine, Keio University, Japan*
[d] *Department of Parasitology, Gunma University Graduate School of Medicine, 3-39-22 Showa-machi, Maebashi, Gunma 371-8511, Japan*

Received 28 June 2006; received in revised form 30 July 2006; accepted 3 August 2006
Available online 18 September 2006

Abstract

To investigate the molecular basis of zymodeme analysis in the enteric protozoan parasite *Entamoeba histolytica*, genes encoding glucose phosphate isomerase (GPI) were isolated from four representative *E. histolytica* strains belonging to zymodeme II, IIα-, XIV, or XIX. Two alleles were obtained from each strain; six alleles with eight polymorphic nucleotide positions were identified among the four strains. Two of these eight polymorphic nucleotides resulted in non-conserved amino acid substitutions. Three GPI isoenzymes with distinct predicted isoelectric points were identified, which agrees well with the observed electrophoretic patterns of GPI from these strains. Amino acid comparisons of GPI from *E. histolytica* and other organisms revealed that all amino acid residues implicated for substrate binding and catalysis were conserved. Biochemical characterization of recombinant *E. histolytica* GPI confirmed that it possessed kinetic parameters similar to GPI from other organisms. The electrophoretic mobility of three GPI isoenzymes was examined by starch gel electrophoresis. Thus, we have established the molecular basis of the classical isoenzymes patterns that have been used for grouping *E. histolytica* isolates and for differentiation of *E. histolytica* from non-pathogenic *Entamoeba dispar*.

Keywords: Glucose phosphate isomerase; *Entamoeba histolytica*; Zymodemes

The protozoan parasite *Entamoeba histolytica* is an etiological agent of amoebiasis, causing an estimated 50 million cases of amebic colitis, dysentery, and extraintestinal abscesses [1] and 40,000–100,000 deaths annually [2]. *E. histolytica*, together with *Giardia intestinalis*, is categorized as a type I amitochondriate protist, which lacks both typical mitochondria and hydrogenosomes [3] and is also deficient in all features of aerobic metabolism. *E. histolytica* produces energy by glycolysis and fermentation under an anaerobic or microaerophilic environment [3,4]. In *E. histolytica*, all enzymes involved in the conversion of glucose into pyruvate by glycolysis have been identified [5,6]. Molecular identification and enzymological characterization of 10 enzymes including hexokinase, inorganic pyrophosphate-dependent phosphofructokinase, and phosphoglucomutase were previously accomplished [7–11]. A recent study by Saarvedra et al. indicated that phosphoglycerate mutase, fructose-1,6-phosphate aldolase, glyceraldehyde-3-phosphate dehydrogenase, and pyruvate phosphate dikinase are flux control steps because they possess the lowest catalytic efficiencies [11]. Four of about a dozen enzymes in the glycolytic pathway, namely hexokinase, phosphoglucomutase, glucose-6-phosphate isomerase (GPI), and malic enzyme, have been used to differentiate *E. histolytica* strains as well as pathogenic *E. histolytica* from non-pathogenic *Entamoeba dispar* species. Although GPI, which is involved in the reversible conversion of glucose-6-phosphate to fructose-6-phosphate, has been used as a gold standard to differentiate the four major groups of *E. histolytica* strains (zymodemes II, IIα-, XIV, and XIX) [12], the molecular basis of this

Abbreviations: GPI, glucose phosphate isomerase; *EhGPI*, *Entamoeba histolytica GPI* gene; EhGPI, *Entamoeba histolytica* glucose phosphate isomerase; ORF, open reading frame; PCR, polymerase chain reaction; rEhGPI, recombinant *E. histolytica* GPI.

☆ Nucleotide sequence data reported in this paper are available in the EMBL, GenBank, and DDJB databases under the accession numbers BAE53444–BAE53451.

* Corresponding author. Tel.: +81 27 220 8020; fax: +81 27 220 8025.
E-mail address: nozaki@med.gunma-u.ac.jp (T. Nozaki).

1383-5769/$ - see front matter © 2006 Elsevier Ireland Ltd. All rights reserved.
doi:10.1016/j.parint.2006.08.001

differentiation has not been established. In this study, we cloned and characterized GPI from representative isolates that belong to four distinct zymodemes (HM1:IMSS cl6, SAW1627, SAW755CR clB, and KU2 for zymodemes II, IIα-, XIV, and XIX, respectively).

A putative *EhGPI* gene of the HM1:IMSS cl6 reference strain was identified in the *E. histolytica* genome database (http://www.tigr.org/tdb/). It contains an open reading frame (ORF) of 1641 nucleotides encoding a protein of 546 amino acids with a predicted molecular mass of 61.4 kDa and pI of 6.91. To examine polymorphisms of GPI sequences in *E. histolytica* strains, the *EhGPI* ORF was amplified by PCR using genomic DNA from the four above-mentioned *E. histolytica* strains with sense (5′-CCTGGATCC*GATG*TTACCAACTCTTCCTGA-3′) and antisense (5′-CCAGGATCC*TTA*GTTTTTTCTCATATC TTTAACA-3′) primers designed based on the sequence information (engineered *Bam*HI sites are underlined, and the start and stop codons are italicized). Conditions and parameters for PCR were previously described [13]. PCR products were digested with *Bam*HI and cloned into *Bam*HI-digested pET-15b (Novagen) in the same orientation as the T7 promoter to produce a GPI fusion protein with a histidine tag at the amino terminus. Six plasmid clones were randomly chosen for each *E. histolytica* strain, and their inserts were sequenced on both strands. Nucleotide sequences of four GPI clones derived from HM1:IMSS cl6 were identical to the sequence in the database (XP 650595 and AAT92031) and the sequence recently reported [11] and were designated "allele 1". The remaining two clones contained four nucleotide substitutions and were designated "allele 2" (Fig. 1A). Similarly, two different alleles of GPI genes were identified from each of the three representative strains of other zymodemes (IIα-, XIV, and XIX) (Fig. 1A). These allelic gene sequences (BAE53444–BAE53451) revealed heterogeneity at eight nucleotide positions. Altogether, six distinct alleles, designated "alleles 1–6" (Fig. 1A), were identified in the four isolates. Two of these nucleotide polymorphisms resulted in non-conserved amino acid substitutions at positions 32 and 449, respectively, and distinct predicted isoelectric points. Isoelectric points of three allelic GPIs (designated isotypes 1–3) varied (isotype 1, 6.91; 2, 7.15; 3, 6.73) (Fig. 1A). However, the total number of amino acids and the predicted molecular mass of all GPIs obtained from these four strains were identical. The predicted pIs of the two allelic gene products in these strains agree well with the observed mobility of GPI isoenzymes in conventional starch gel electrophoresis, assuming that *E. histolytica* GPI forms homo- and heterodimers as previously shown in other organisms (e.g., [14]).

To further examine features of *E. histolytica* GPIs (EhGPIs), they were compared with homologs from archaea, bacteria, fungi, protists, plants, and metazoa, revealing 30–64% identity to EhGPI (representative species are shown in Fig. 1B). EhGPIs showed 44–60% identity to GPIs from *Escherichia coli*, *Aspergillus oryzae*, *Homo sapiens*, and *Spinacia oleracea*. EhGPIs showed 41–54% identity to GPIs from other parasitic protists including *Leishmania mexicana*, *Trypanosoma brucei*,

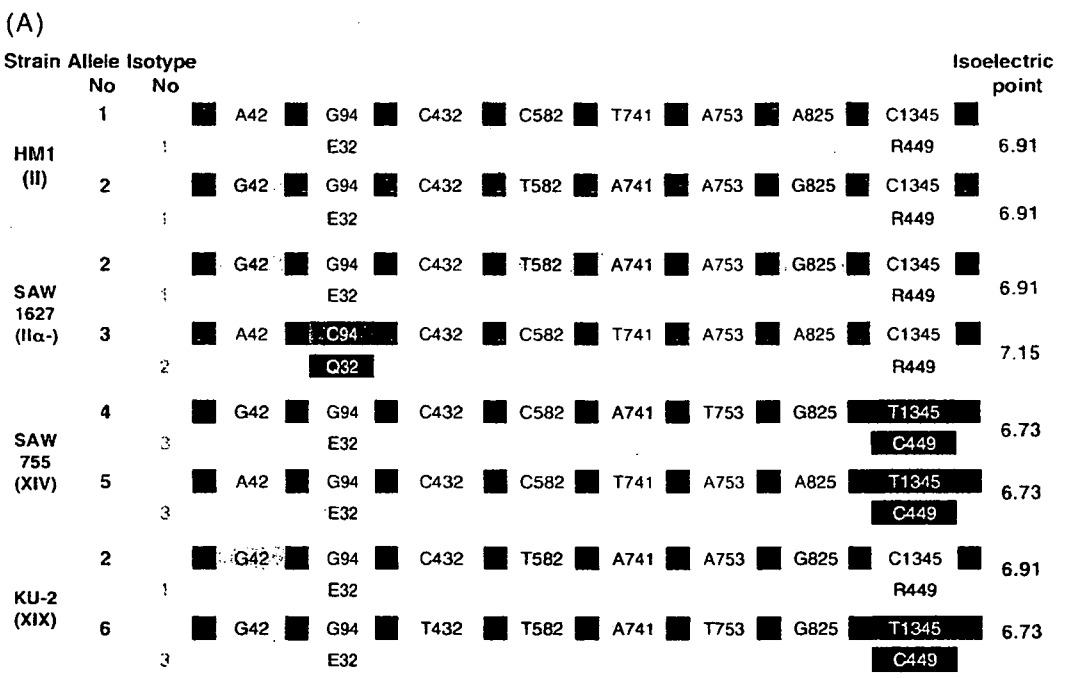

Fig. 1. Comparison of GPI nucleotide and protein sequences. (A) Schematic representation of nucleotide (top) and amino acid (bottom) sequences of two GPI alleles in four representative *E. histolytica* strains. Only nucleotides and amino acids showing heterogeneity are indicated, with predicted pI values. (B) Multiple alignments of deduced amino acid sequences of GPIs from *E. histolytica* and other organisms. Protein primary structures were aligned using the CLUSTAL W program version 1.83 (http://www.ddbj.nig.ac.jp/search/clustalw-e.html) with the BLOSUM matrix. Sequences are *Entamoeba histolytica* (Eh), *Homo sapiens* (Hs), *Escherichia coli* (Ec), *Trypanosoma cruzi* (Tc), *T. brucei* (Tb), *Leishmania mexicana* (Lm), *Aspergillus oryzae* (Ao), *Plasmodium falciparum* (Pf), *Toxoplasma gondii* (Tg), *Spinacia oleracea* (So), *Giardia intestinalis* (Gi), and *Trichomonas vaginalis* (Tv). Asterisks indicate identical amino acids. Dots and colons indicate conserved amino acids substitutions. Dashes indicate computer-generated gaps. Residues deduced from crystal structures (16–18) to be important for substrate binding and/or catalysis of GPIs are shaded in black, and the two signature patterns of the GPI family, [DENS]-X-[LIVM]-G-G-R-[FY]-S-[LIVMT]-X-[STA]-[PSAC]-[LIVMA]-G and [GS]-X-[LIVM]-[LIVMFYW]-XXXX-[FY]-[DN]-Q-X-G-V-E-X-X-K, are highlighted by gray boxes.

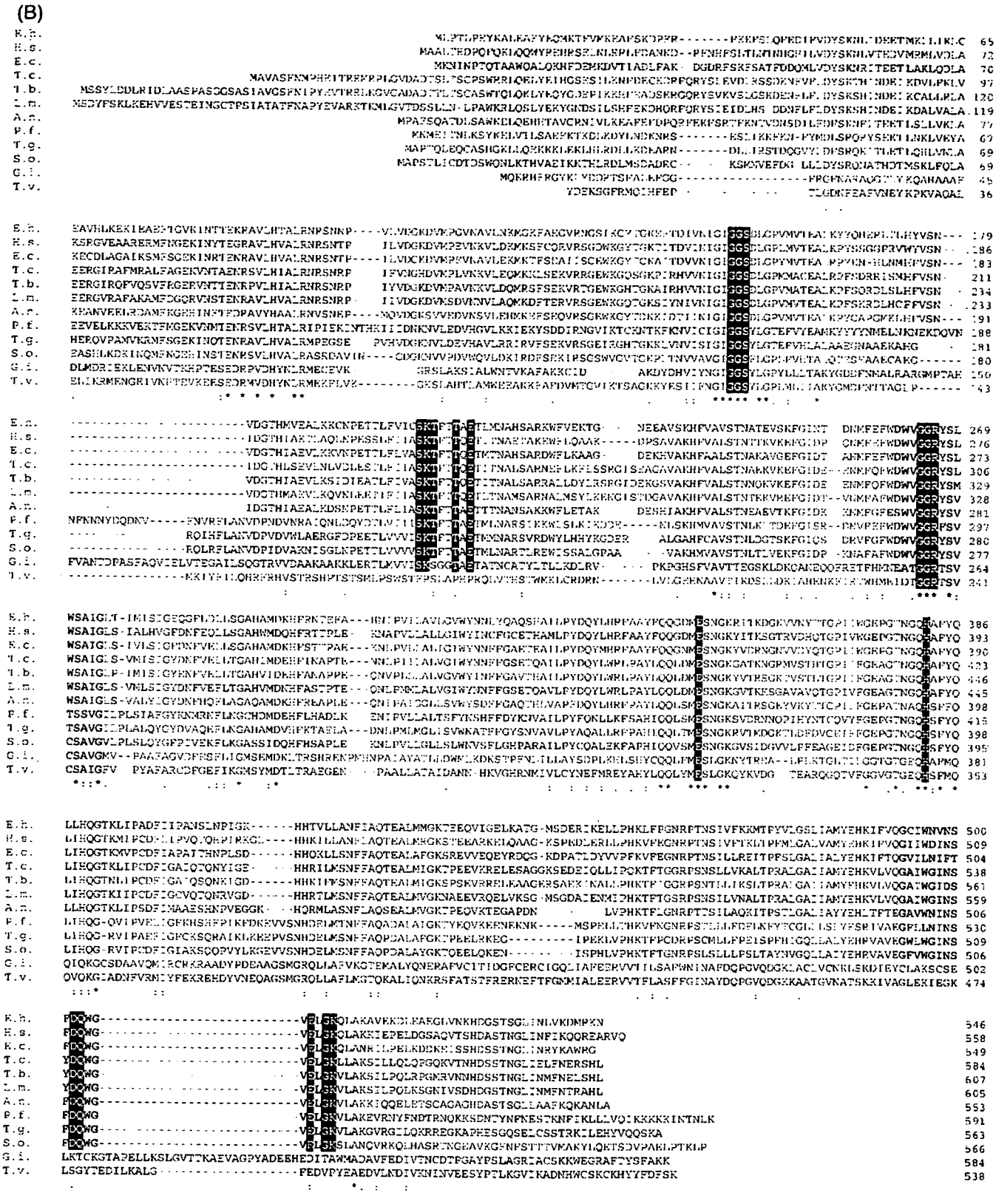

Fig. 1 (*continued*).

Trypanosoma cruzi, *Toxoplasma gondii*, and *Plasmodium falciparum*, while their similarity to representative amitochondriate and microaerophilic/anaerobic protists *Trichomonas vaginalis* and *G. intestinalis* was lower (31–32% identity). This finding suggests distinct GPI ancestors for these amitochondriate parasites, which was also supported by the

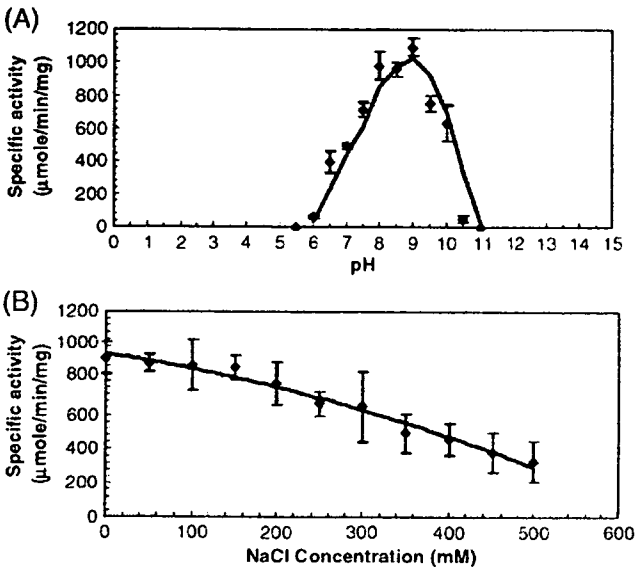

Fig. 2. (A) pH dependence of *E. histolytica* GPI. The pH optimum of the enzyme was determined in the direction of glucose-6-phosphate formation from fructose-6-phosphate between pH 5.5 and 11 at 25 °C in a coupling assay. The 100-μl assay mixture was comprised of 100 mM either 2-Morpholinoethanesulfonic acid (pH 5.5, 6.0, and 6.5), *N*-(2-hydroxyethyl)piperazine-*N'*-(2-ethanesulfonic acid) (pH 7.0, 7.5, and 8.0), *N*-[Tris(hydroxymethyl)methyl]-3-aminopropanesulfonic acid (pH 8.5, 9.0, and 9.5), or 3-(cyclohexylamino)-1-propanesulfonic acid (pH 10, 10.5, and 11); 2 mM fructose-6-phosphate; 0.5 mM NADP; 0.1 U glucose-6-phosphate dehydrogenase; and 0.1 μg purified EhGPI protein. Error bars represent standard errors from three independent experiments. (B) The effect of NaCl on EhGPI activity. The activity of EhGPI was determined in a 100-μl assay mixture comprised of 100 mM TAPS, pH 9.0; 2 mM fructose-6-phosphate; 0.5 mM NADP; 0.1 U glucose-6-phosphate dehydrogenase; and 0.1 μg purified EhGPI protein, with the addition of 0–500 mM NaCl. Error bars represent standard errors from five independent experiments.

previous phylogenetic study [15]. Two conserved signature patterns of GPI [16,17] are totally conserved in EhGPIs (Fig. 1B). In addition, all conserved residues that were shown by various crystal structures or mutagenesis studies [18–20] to be crucial for substrate recognition, binding, or catalysis are highly conserved in EhGPI (Fig. 1B). For instance, the following amino acid residues are completely conserved: Thr205, Thr208, Ser153, Ser203, and Lys204 (numbering based on EhGPI), crucial for binding to the phosphate group; His382, Lys510, Glu210, Ile150, Thr378, Glu507, Arg266, Asp502, Gln503, and Glu351, essential for catalysis; and Gly151, Gly152, Gly264, and Gly265, involved in substrate specificity. EhGPIs lack the long amino-terminal extension present in GPIs from *L. mexicana*, *T. cruzi*, and *T. brucei* that is involved in targeting the enzyme to glycosomes [21]. This is consistent with the premise that EhGPI is cytosolic. EhGPI also lacks an internal insertion (between amino acids 227 and 228) present in GPIs from *L. mexicana*, *T. cruzi*, and *T. brucei*, a 27-amino-acid amino-terminal extension in *G. intestinalis* GPI, and a long carboxyl-terminal extension present in GPI from *T. vaginalis* and *G. intestinalis* [22].

To investigate biochemical features of EhGPIs, the recombinant EhGPIs corresponding to three representative proteins [EhGPI isotypes 1–3, which represent allele 1 of HM1:IMSS cl6 (BAE53444), allele 3 of SAW1627 (BAE53447), and allele 4 of SAW755CR clB (BAE53448)] were produced using a prokaryotic expression system and purified as previously described [23]. Upon SDS-polyacrylamide gel electrophoresis, the recombinant EhGPI (rEhGPI) proteins appeared as an apparently homogeneous single band of approximately 63 kDa, which agrees with the predicted size of a monomeric EhGPI protein with an additional stretch of 21 amino acids at the amino terminus. The formation of glucose-6-phosphate from fructose-6-phosphate in the reverse reaction catalyzed by rEhGPI was measured by monitoring the reduction of $NADP^+$ spectrophotometrically at 340 nm [24]. rEhGPI isotype 1 was active over a wide pH range (7.0–10.0) with optimal pH of 8.0–9.0 (Fig. 2A), consistent with the previous study [11]. GPI activity was inhibited by addition of a monovalent cation (e.g., Na^+) (Fig. 2B), similar to GPI from *Aspergillus niger* [25]. rEhGPI followed Michaelis–Menten kinetics. Kinetic constants under the standard assay conditions (containing 25–300 μM substrates; see Fig. 2 legend for details) were determined with Lineweaver-Burk plots. rEhGPI showed a K_m value of 122±16 μM for fructose-6-phosphate and a specific activity of 786±59 μmol min^{-1} mg $protein^{-1}$ in the reverse reaction, which are of the same order of magnitude as those determined in the previous study (V_{max}, 620 μmol min^{-1} mg $protein^{-1}$; K_m, 480 μM; measured at pH 8 and 37 °C) [11]. The K_m and specific activity of rEhGPI were comparable to GPI from other organisms, e.g., *A. niger* [25], *L. mexicana* [21,26], *T. cruzi* [27], *T. brucei* [26,28], and rabbit [28].

To establish the relationship between individual GPI isotypes identified in this study and zymodemes revealed by starch gel electrophoresis in four representative *E. histolytica* strains, we examined both native and recombinant GPI isoenzymes using starch gel electrophoresis. The electrophoretic mobilities of native and recombinant GPI isoenzymes were similar despite marginal differences in molecular mass and isoelectric point due to the amino-terminal addition of the histidine tag (plus 2.4 kDa; 6.91 vs. 6.88, 7.15 vs. 7.04, and 6.73 vs. 6.74 for EhGPI isotypes 1–3, respectively) (data not shown), confirming that isoenzyme profiles displayed by starch gel electrophoresis reflect two allelic GPI isotypes. Although zymodeme XIX showed the three expected bands on the starch gel, the mixture of recombinant GPI isotypes 1 and 3 gave rise to only two bands corresponding to two homodimers (isotypes 1/1 and 3/3) (data not shown). This is consistent with the hypothesis that a heterodimer (composed of isotypes 1 and 3) is not efficiently formed unless two GPI isotypes are simultaneously synthesized in vivo. These results may also indicate that the homodimers are structurally stable.

These data demonstrate for the first time the molecular basis of classical isoenzyme patterns that have been used for the characterization of *E. histolytica* isolates by zymodeme analyses, considered the "gold standard" to differentiate *E. histolytica* strains as well as pathogenic from non-pathogenic species [12,29]. Our results, together with the allelic heterogeneity of hexokinase and phosphoglucomutase [7–10], indicate that isoenzyme profiles are primarily, if not solely, attributable to sequence diversities at the primary sequence level. Our data further enable the establishment of PCR-based zymodeme analysis that

can replace laborious and time-consuming zymodeme analysis using starch gel electrophoresis.

Acknowledgments

The authors express their appreciation to Vahab Ali, Gunma University; Yasuo Shigeta and Yumiko Saito-Nakano, National Institute of Infectious Diseases, Japan; Bahram Kazemi, Shaheed Beheshti University of Medical Sciences; and Bijan Farzami, Tehran University of Medical Sciences for technical assistance and helpful discussions. This work was supported in part by a Grant-in-Aid for Scientific Research from the Ministry of Education, Culture, Sports, Science, and Technology of Japan to T.N.; a grant for Research on Emerging and Re-emerging Infectious Diseases from the Ministry of Health, Labor, and Welfare; a grant for the Project to Promote the Development of Anti-AIDS Pharmaceuticals from the Japan Health Sciences Foundation to T.N.; a fellowship from Japan Society for the Promotion of Science to A.H.; a scholarship from The Ministry of Health, Treatment, and Medical Education of Iran to E.R.; and financial support from Tehran University to M.R.

References

[1] Gilchrist CA, Petri WA. Virulence factors of *Entamoeba histolytica*. Curr Opin Microbiol 1999;2:433–7.

[2] WHO/UNESCO Report. A consultation with experts on amoebiasis. Epidemiol Bull 1997;18:13–4.

[3] Müller M. Enzymes and compartmentation of core energy metabolism of anaerobic protists—a special case in eukaryotic evolution. In: Coombs GH, Vickerman K, Sleigh MA, Warren A, editors. Evolutionary Relationships among Protozoa. The Netherlands: Kluwer Academic Publishers; 1998. p. 109–32.

[4] Reeves RE. Metabolism of *Entamoeba histolytica* Schaudinn. Adv Parasitol 1903;23:105–42.

[5] Loftus B, Anderson I, Davies R, Alsmark UC, Samuelson J, Amedeo P, et al. The genome of the protist parasite *Entamoeba histolytica*. Nature 2005;433:865–8.

[6] Anderson IJ, Loftus BJ. *Entamoeba histolytica*: observations on metabolism based on the genome sequence. Exp Parasitol 2005;110:173–7.

[7] Ortner S, Plaimauer B, Binder M, Scheiner O, Wiedermann G, Duchene M. Molecular analysis of two hexokinase isoenzymes from *Entamoeba histolytica*. Mol Biochem Parasitol 1995;73:189–98.

[8] Ortner S, Clark CG, Binder M, Scheiner O, Wiedermann G, Duchene M. Molecular biology of the hexokinase isoenzyme pattern that distinguishes pathogenic *Entamoeba histolytica* from nonpathogenic *Entamoeba dispar*. Mol Biochem Parasitol 1997;86:85–94.

[9] Ortner S, Binder M, Scheiner O, Wiedermann G, Duchene M. Molecular and biochemical characterization of phosphoglucomutases from *Entamoeba histolytica* and *Entamoeba dispar*. Mol Biochem Parasitol 1997;90:121–9.

[10] Kroschewski H, Ortner S, Steipe B, Scheiner O, Wiedermann G, Duchene M. Differences in substrate specificity and kinetic properties of the recombinant hexokinases HXK1 and HXK2 from *Entamoeba histolytica*. Mol Biochem Parasitol 2000;105:71–80.

[11] Saavedra E, Encalada R, Pineda E, Jasso-Chavez R, Moreno-Sanchez R. Glycolysis in *Entamoeba histolytica*. Biochemical characterization of recombinant glycolytic enzymes and flux control analysis. FEBS J 2005;272:1767–83.

[12] Sargeaunt PG, Williams JE, Grene JD. The differentiation of invasive and non-invasive *Entamoeba histolytica* by isoenzyme electrophoresis. Trans R Soc Trop Med Hyg 1978;72:519–21.

[13] Nozaki T, Asai T, Sanchez LB, Kobayashi S, Nakazawa M, Takeuchi T. Characterization of the gene encoding serine acetyltransferase, a regulated enzyme of cysteine biosynthesis from the protist parasite *Entamoeba histolytica* and *Entamoeba dispar*: regulation and possible function of the cysteine biosynthetic pathway in *Entamoeba*. J Biol Chem 1999;274:32445–52.

[14] Van Beneden RJ, Powers DA. Structural and functional differentiation of two clinally distributed glucose phosphate isomerase allelic isozymes from the teleost *Fundulus heteroclitus*. Mol Biol Evol 1989;6:155–70.

[15] Huang J, Mullapudi N, Lancto CA, Scott M, Abrahamsen MS, Kissinger JC. Phylogenomic evidence supports past endosymbiosis, intracellular and horizontal gene transfer in *Cryptosporidium parvum*. Genome Biol 2004;5:R88.

[16] Sun YJ, Chou CC, Chen WS, Wu RT, Meng M, Hsiao CD. The crystal structure of a multifunctional protein: phosphoglucose isomerase/autocrine motility factor/neuroleukin. Proc Natl Acad Sci U S A 1999;96:5412–7.

[17] Hansen T, Oehlmann M, Schonheit P. Novel type of glucose-6-phosphate isomerase in the hyperthermophilic archaeon *Pyrococcus furiosus*. J Bacteriol 2001;183:3428–35.

[18] Lee JH, Chang KZ, Patel V, Jeffery CJ. Crystal structure of rabbit phosphoglucose isomerase complexed with its substrate D-fructose 6-phosphate. Biochemistry 2001;40:7799–805.

[19] Jeffery CJ, Hardre R, Salmon L. Crystal structure of rabbit phosphoglucose isomerase complexed with 5-phospho-D-arabinonate identifies the role of Glu357 in catalysis. Biochemistry 2001;40:1560–6.

[20] Cordeiro AT, Godoi PH, Silva CH, Garratt RC, Oliva G, Thiemann OH. Crystal structure of human phosphoglucose isomerase and analysis of the initial catalytic steps. Biochim Biophys Acta 2003;1645:117–22.

[21] Cordeiro AT, Michels PA, Delboni LF, Thiemann OH. The crystal structure of glucose-6-phosphate isomerase from *Leishmania mexicana* reveals novel active site features. Eur J Biochem 2004;271:2765–72.

[22] Henze K, Horner DS, Suguri S, Moore DV, Sanchez LB, Muller M, et al. Unique phylogenetic relationships of glucokinase and glucose phosphate isomerase of the amitochondriate eukaryotes *Giardia intestinalis*, *Spironucleus barkhanus* and *Trichomonas vaginalis*. Gene 2001;281:123–31.

[23] Ali V, Shigeta Y, Tokumoto U, Takahashi Y, Nozaki T. An intestinal parasitic protist *Entamoeba histolytica* possesses a non-redundant NIF-like system for iron–sulfur cluster assembly under anaerobic conditions. J Biol Chem 2004;279:16863–74.

[24] Jeong JJ, Fushinobu S, Ito S, Jeon BS, Shoun H, Wakagi T. Characterization of the cupin-type phosphoglucose isomerase from the hyperthermophilic archaeon *Thermococcus litoralis*. FEBS Lett 2003;535:200–4.

[25] Ruijter GJ, Visser J. Characterization of *Aspergillus niger* phosphoglucose isomerase. Use for quantitative determination of erythrose 4-phosphate. Biochimie 1999;81:267–72.

[26] Nyame K, Do-Thi CD, Opperdoes FR, Michels PA. Subcellular distribution and characterization of glucose phosphate isomerase in *Leishmania mexicana mexicana*. Mol Biochem Parasitol 1994;67:269–79.

[27] Concepcion JL, Chataing B, Dubourdieu M. Purification and properties of phosphoglucose isomerases of *Trypanosoma cruzi*. Comp Biochem Physiol B Biochem Mol Biol 1999;122:211–22.

[28] Marchand M, Kooystra U, Wierenga RK, Lambeir AM, Van Beeumen J, Opperdoes FR, et al. Glucose phosphate isomerase from *Trypanosoma brucei*. Cloning and characterization of the gene and analysis of the enzyme. Eur J Biochem 1989;184:455–64.

[29] Sargeaunt PG. Zymodemes of *Entamoeba histolytica*. In: Ravdin JI, editor. Amoebiasis: human infection by *Entamoeba histolytica*. New York: John Wiley and Jone Inc; 1988. p. 370–87.

Available online at www.sciencedirect.com
SCIENCE DIRECT
ELSEVIER
Molecular & Biochemical Parasitology 145 (2006) 216–225
MOLECULAR & BIOCHEMICAL PARASITOLOGY

Characterization of protein geranylgeranyltransferase I from the enteric protist *Entamoeba histolytica*☆

Asao Makioka[a], Masahiro Kumagai[a], Tsutomu Takeuchi[b], Tomoyoshi Nozaki[c,d,*]

[a] *Department of Tropical Medicine, Jikei University School of Medicine, 3-25-8 Nishi-shinbashi, Minato-ku, Tokyo 105-8461, Japan*
[b] *Department of Tropical Medicine and Parasitology, Keio University School of Medicine, 35 Shinanomachi, Shinjuku-ku, Tokyo 160-8582, Japan*
[c] *Department of Parasitology, Gunma University Graduate School of Medicine, 3-39-22 Showa-machi, Maebashi, Gunma 371-8511, Japan*
[d] *Precursory Research for Embryonic Science and Technology, Japan Science and Technology Agency, 2-20-5 Akebonocho, Tachikawa, Tokyo 190-0012, Japan*

Received 23 August 2005; received in revised form 28 September 2005; accepted 4 October 2005
Available online 19 October 2005

Abstract

Entamoeba histolytica is a unique protozoan parasite possessing both protein farnesyltransferase and geranylgeranyltrasferase I (GGT-I) for isoprenylation of small GTPases. In this study, we demonstrated unique enzymological properties of the amebic GGT-I (*Eh*GGT-I), including substrate specificity and insensitivity to known mammalian inhibitors. Some of important residues of the catalytic β subunit implicated in the specificity for GTPase acceptors and prenyl donors are substituted in *Eh*GGT-I. Recombinant α and β subunits of *Eh*GGT-I, co-expressed in *Escherichia coli*, showed activity to transfer geranylgeranyl to both human wild-type (CVLS) and mutant (CVLL) H-Ras, while the mammalian GGT-I geranylgeranylated, but not farnesylated, only mutant H-Ras. All the representative amebic Ras and Rho/Rac small GTPases with phenylalanine, leucine, methionine, or alanine terminus were preferentially geranylgeranylated by *Eh*GGT-I. This indicates that the acceptor specificity of the amebic GGT-I is remarkably broader than that of its mammalian counterpart. In contrast to *Eh*FT, which farnesylates but not geranylgeranlylates solely *Eh*Ras4-CVVA, *Eh*GGT-I also showed significant farnesyltransferase activity against Ras GTPase acceptors. *Eh*GGT-I showed remarkable resistance to peptidomimetics known to inhibit mammalian GGT-I. Together with our previous observation that this parasite does not appear to depend on farnesylation for a majority of Ras and Rho/Rac, these data indicate that biological and biochemical advantages leading to the evolutional selection of this isoprenyl modification must exist uniquely in this parasitic protist. Finally, remarkable biochemical differences in binding to substrates and inhibitors between amebic and mammalian GGT-I highlight this enzyme as an attractive target for the development of new chemotherapeutics against amebiasis.

Keywords: *Entamoeba histolytica*; Protein prenylation; Protein geranylgeranyltransferase I; Protein farnesyltransferase; Ras superfamily small GTPases

1. Introduction

Protein geranylgeranyltransferase type I (GGT-I; E.C. 2.5.1.59) and a closely related protein, farnesyltransferase (FT), are prenyl enzymes responsible for geranylgeranylation and farnesylation, respectively, which are major posttranslational lipid modifications of proteins including small GTPases of the Ras superfamily [1]. The isoprenylation of small GTPases is required for membrane association and their function in signal transduction involved in cell proliferation, differentiation and intracellular membrane trafficking [1–3]. GGT-I and FT, which are also called as CaaX prenyltransferases [4], catalyze

Abbreviations: GGT-I, protein geranylgeranyltrasferase I; *Eh*GGT-I, *Entamoeba histolytica* GGT-I; FT, protein farnesyltransferase; GGPP, geranylgeranyl pyrophosphate; FPP, farnesyl pyrophosphate; GGT-Iα, α subunit of GGT-I; GGT-Iβ, β subunit of GGT-I; SDS-PAGE, sodium dodecyl sulfate-polyacrylamide gel electrophoresis; NTA, Ni-nitrilotriacetic acid

☆ *Note:* The nucleotide sequence data of *Entamoeba histolytica* GGT-Iβ reported in this paper has been submitted to the DDBJ/GenBank®/EBI data bank with Accession number AB161971.

* Corresponding author. Tel.: +81 27 220 8020; fax: +81 27 220 8025.
E-mail address: nozaki@med.gunma-u.ac.jp (T. Nozaki).

0166-6851/$ – see front matter © 2005 Elsevier B.V. All rights reserved.
doi:10.1016/j.molbiopara.2005.10.005

the transfer of the geranylgeranyl and farnesyl group from geranylgeranyl pyrophosphate (GGPP) and farnesyl pyrophosphate (FPP), respectively, to the cysteine residue of a carboxyl-terminal CaaX of small GTPases including Ras, Rac, Rho, and Rap, where C, a, or X is cysteine, an aliphatic amino acid, or any amino acid, respectively. Mammalian FT or GGT-I generally prefers substrates including small GTPases possessing a terminal CaaX, where X is one of the following amino acids: Cys, Ser, Gln, Ala, Met, Thr, His, Val, Asn, Phe, Gly, or Ile for FT and Leu, Phe, Ile, Val, or Met for GGT-I in the order of decreasing affinity [5]. However, exceptions have been described in various organisms: e.g. K-RasB-CVIM is isoprenylated by both FT and GGT-I [6]. These data suggest the presence of not-yet-identified mechanistic details determining the substrate preferences of these isoprenyl enzymes. The third enzyme, GGT-II, transfers the geranylgeranyl groups from GGPP to both cysteine residues of CC- or CXC-containing proteins almost exclusively composed of members of the Rab family small GTPases [1].

Mutations in Ras, which correlate with cellular transformation and tumor development, have been found in nearly 30% of all human cancers [7]. Oncogenic Ras proteins have been shown to require farnesylation for their ability to transform cells [1]. Consequently, FT has been attracting attention as a target of cancer chemotherapy [8]. FT inhibitors have also been found to be effective against parasitic infections such as African sleeping sickness caused by *Trypanosoma brucei* and malaria caused by *Plasmodia* species [9]. Although GGT-I has drawn less attention than FT, GGT-I inhibitors are also viewed as potential anticancer agents because K-RasB, the most commonly mutated form of Ras, has often been shown to be geranylgeranylated as well as farnesylated [6]. Furthermore, a number of studies have shown that GGT-I inhibitors are effective against tumor progression [10] and smooth muscle hyperplasia [11].

Entamoeba histolytica is the intestinal protozoan parasite that causes amebic dysentery, colitis, and liver abscess in humans, and is responsible for an estimated 50 million cases of amebiasis and 40–100 thousand deaths annually [12]. A number of small GTPases of this parasite have been studied including Ras/Rap [13,14], Rho/Rac [15–19], and Rab [20–23], and the molecular and cellular functions of some of these small GTPases are beginning to be unveiled [13,18,19,23–25]. To elucidate the prenylation of these small GTPases in *E. histolytica*, we previously cloned genes encoding the α- and β-subunits of FT of this parasite and characterized the FT recombinant enzyme, which revealed remarkable biochemical differences in binding to substrates and inhibitors from mammalian FT [26]. We showed that the amebic FT did not utilize a majority of Ras and Rap as a substrate, but specifically farnesylated only a single Ras isotype, Ras4, which possesses an unusual primary structure. However, the molecular and biochemical identity of an enzyme (or enzymes) responsible for the isoprenylation of the remaining Ras and Rap proteins in this organism remains unknown.

To better understand the peculiarity of substrate selection of isoprenylation enzymes in this parasitic protozoon, we characterized GGT-I from *E. histolytica* (*Eh*GGT-I) in this study. We show that *Eh*GGT-I exhibits activity against a wide spectrum of small GTPases of *E. histolytica*, which is in marked contrast to *Eh*FT. We also show remarkable differences in substrate specificity and sensitivity against known peptidomimetic inhibitors of mammalian GGT-I between *Eh*GGT-I and rat GGT-I, indicating amebic GGT-I to be an ideal target for the development of new chemotherapeutics against amebiasis.

2. Materials and methods

2.1. Parasite

Trophozoites of *E. histolytica* strain HM:IMSS cl6 [27] were cultured axenically in BI-S-33 medium at 35.5 °C [28].

2.2. Chemicals

Recombinant rat GGT-I, recombinant human H-Ras-CVLS (wild type), H-Ras-CVLL (mutant), and peptidomimetic inhibitors GGTI-287 (*N*-4-[2 (*R*)-amino-3-mercatopropyl] amino-2-phenylbenzoyl-(L)-leucine trifluoroacetate) and GGTI-297 (*N*-4-[2(*R*)-amino-3-mercatopropyl]amino-2-naphthylbenzoyl-(L)-leucine trifluoroacetate) were purchased from EMD Biosciences (La Jolla, CA). [^{3}H] geranylgeranyl pyrophosphate (23.0 Ci/mmol) and [^{3}H] farnesyl pyrophosphate (16.1 Ci/mmol) were purchased from Perkin-Elmer Life Sciences (Boston, MA). Restriction endonucleases and modifying enzymes were purchased from Takara Biochemical (Tokyo, Japan). The other chemicals and reagents were purchased from either Sigma–Aldrich Fine Chemicals (St. Louis, MO) or Wako Pure Chemical Industries (Osaka, Japan) unless otherwise mentioned and were of the highest purity available.

2.3. cDNA library of E. histolytica

A trophozoite cDNA library of *E. histolytica* was constructed using the poly(A)$^+$ RNA and λZAP II phage (Stratagene, La Jolla, CA) as described previously [29].

2.4. Identification and cloning of GGT-Iβ of E. histolytica

We designed oligonucleotide primers to amplify the protein-coding region of the GGT-I β subunit from *E. histolytica* by PCR based on a homology search using yeast and mammalian GGT-I against the *E. histolytica* genome database available at The Institute for Genomic Research (http://www.tigr.org/tdb/). The sense and antisense primers for *Eh*GGT-Iβ were 5′-ATGAATGCACCTAATTTAAGAAGTGAAG-3′ and 5′-TCAAAGATATGATGGTTTTTCAATTCC-3′, respectively. PCR was performed using a one-hundredth volume of the cDNA phage lysate as a template with the following parameters. The initial step of denaturation at 94 °C for 3 min was followed by 30 cycles of denaturation at 94 °C for 1 min, annealing at 55 °C for 2 min, and extension at 72 °C for 2 min. The final step at 72 °C for 10 min was added to complete the extension. The amplified DNA fragments were electrophoresed, purified using a Geneclean II kit (BIO101, La Jolla, CA) and used as templates for subsequent PCR (see below). Since FT and GGT-I share their α subunit in all the organisms so far analyzed, we utilized the α subunit of

E. histolytica FT [26] as the GGT-I α subunit. Thus, the term "GGT-I α subunit" is synonymous with "FT α subunit" in this study. The nucleotide sequences reported in this paper have been submitted to the DDBJ/GenBank™/EBI Data Bank with accession number AB161971 (GGT-Iβ of *E. histolytica*).

2.5. Construction of a plasmid to express recombinant EhGGT-I

A plasmid containing the protein-coding regions of GGT-Iα (without the stop codon), GGT-Iβ (with the stop codon), and the ribosome-binding sequence (GAGGAGTTTTAACTT) between them was constructed by three rounds of PCR [30,31]. Briefly, a set of initial-round PCRs were conducted to amplify the GGT-Iα and GGT-Iβ protein-coding region using a sense primer, 5′-ATGGAAGAAGACGAAGAAATCACATTTG-3′, and an antisense primer, 5′-ATGATTAGTAATTTTTGTTAAATACCAATCCC-3′ (for GGT-Iα), and using a sense primer, 5′-ATGAATGCACCTAATTTAAGAAGTGAAG-3′, and an antisense primer, 5′-TCAAAGATATGATGGTTTTTCAATTCC-3′ (for GGT-Iβ), respectively. The second PCR was conducted using the respective product of the first reaction as a template. To amplify the GGT-Iα protein-coding region (excluding the stop codon) flanked by a *Bam*HI site (italicized) and the ribosome-binding site (underlined), a sense primer, 5′-GGA*GGATCC*CATGGAAGAAGACGAAGAAATCACATTTG-3′ (primer 1) and an antisense primer, 5′-AAGTTAAAACTCCTCATGATTAGTAATTTTTGTTAAATACCAATCCC-3′ were used. To amplify the GGT-Iβ sequence including the stop codon, flanked by the ribosome-binding site (underlined) and a *Hin*dIII site (italicized), a sense primer, 5′-GAGGAGTTTTAACTTATGAATGCACCTAATTTAAGAAGTGAAG-3′, and an antisense primer, 5′-CCA*AAGCTT*TCAAAGATATGATGGTTTTTCAATTCC-3′ (primer 2), were used. The third round of PCR was conduced using a mixture of the products of the second round, and primers 1 and 2. The resulting 2-kb PCR product was digested with *Bam*HI and *Hin*dIII and ligated into *Bam*HI, and *Hin*dIII double-digested pQE31 (QIAGEN, Hilden, Germany) to construct pEhGGT-Iαβ. Nucleotide sequences were confirmed with an ABI Prism BigDye terminator cycle sequencing ready reaction kit (PE Applied Biosystems, Foster City, CA) on an ABI Prism 310 Genetic Analyzer. In pEhGGT-Iαβ, the GGT-Iα and GGT-Iβ protein-coding regions placed in tandem were presumably translationally coupled, facilitating the co-expression of these two subunits at similar levels. An amino-terminal histidine tag was also engineered in pEhGGT-Iα to facilitate purification.

2.6. Construction of plasmids to express recombinant small GTPases

Construction of plasmids for *Eh*Rasl-4 and *Eh*RacC were previously described [26]. Similarly, a protein-coding region of *Eh*RacA, *Eh*RacG, and *Eh*Rapl-2 flanked by additional *Bam*HI and *Sal*I sites (italicized) were amplified by PCR using cDNA as a template and the following sense and antisense primers: 5′-GGA*GGATCC*CATGCAAGCTGTCAAATGTGT-3′ and 5′-CCAGT*CGAC*TTAGAATAATAAACATCCTCT-3′ (*Eh*RacA); 5′-GGA*GGATCC*CATGAGACCAGTGAAACTTGT-3′ and 5′-CCA*GTCGAC*TTAGAATAATGAGCATCCTTT-3′ (*Eh*RacG); 5′-GGA*GGATCC*CATGCCAGTAAAAGACTATAAAATTGTAGTA-3′ and 5′-CCA*GTCGAC*TTAGAGAAGAGAACAATGATGAGCATGATC-3′ (*Eh*Rapl); 5′-GGA*GGATCC*CATGCCAGTGAAAGACTACAAAATTGTAGTA-3′ and 5′-CCA*GTCGAC*TTAGAAGAGAGAACATCCACCACTCTTCTT-3′ (*Eh*Rap2), where the restriction sites are italicized. PCR products were electrophoresed, purified, and cloned into *Bam*HI, and *Sal*I double-digested pQE31 plasmid to obtain pEhRacA, pEhRacG, pEhRapl and pEhRap2. The resulting plasmids were designed to express proteins containing an amino-terminal histidine tag to facilitate purification.

2.7. Expression and purification of recombinant proteins

Plasmids constructed as described above were introduced into *Escherichia coli* M15 cells. A 12 ml seed culture was grown overnight at 37 °C in LB medium containing 100 μg/ml ampicillin and 25 μg/ml kanamycin. The overnight culture was then inoculated into 250 ml of fresh medium containing the antibiotics. The bacteria were grown for 1 h, and then for another 4 h after the addition of 1 mM isopropyl β-D-thiogalactopyranoside to induce protein expression. The bacteria were harvested by centrifugation at 4000 × *g* for 20 min, and the pellet was stored at −20 °C until purification. The recombinant proteins were purified according to the manufacturers' instructions. Briefly, the bacterial cells were resuspended in cold lysis buffer, phosphate-buffered saline (PBS), pH 8.0, containing 10 mM imidazole and 1% lysozyme, sonicated, and centrifuged at 10,000 × *g* for 20 min. The supernatant was applied to a Ni-NTA agarose column (QIAGEN), washed extensively with the wash buffer containing 20 mM imidazole, and eluted with the lysis buffer containing 250 mM imidazole. The purified recombinant GGT-I and small GTPase proteins were then dialyzed against the enzyme assay buffer described below and 40 mM Tris–HCl, pH 8, containing 90 mM NaCl, 10 mM $MgCl_2$ and 2 mM dithiothreitol (DTT) and stored with 20 and 50% glycerol, respectively, at −80 °C until use. After purification, recombinant *Eh*GGT-I was estimated to be >95% pure by densitometric quantitation. Protein concentrations were determined by the method of Bradford [32] using Protein Assay CBB solution (Nacalai Tesque, Kyoto, Japan). Bovine serum albumin was used as the protein standard.

2.8. Sequence analysis

GGT-Iβ and FTβ protein sequences from *E. histolytica* and 16 other organisms were retrieved from the databases available at TIGR and the National Center for Biotechnology Information (http://www.ncbi.nih.gov/) using the BLASTP and TBLASTN algorithms. The protein alignment and phylogenetic analyses were performed with CLUSTAL W version 1.81 [33] using the Neighbor-joining (NJ) method [34] with the Blosum matrix created using the CLUSTAL W program [33]. Unrooted NJ trees

were drawn with TreeView version 1.6.0 [35]. Branch lengths and bootstrap values (1000 replicates) [36] were derived from the NJ analysis.

2.9. Protein analyses

The expression and purity of recombinant proteins were evaluated by standard sodium dodecyl sulfate-polyacrylamide gel electrophoresis (SDS-PAGE) as described [37]. To prepare *E. histolytica* extracts, trophozoites were washed three times with ice cold PBS, resuspended at 10^7 ml^{-1} in PBS containing a proteinase inhibitor cocktail [1 mM phenylmethylsulfonyl fluoride, 1 nM trypsin inhibitor, 100 μM trans-epoxysuccinyl-L-leucylamino-(4-guanidino) butane, 1 μg/ml pepstatin A, 1 μg/ml leupeptin, 1 μg/ml *N*-α-p-tosyl-L-lysine chloromethyl ketone hydrochloride, and 1 mM benzamidine hydrochloride], and subjected to three cycles of freezing and thawing. After centrifugation at 10,000 × *g* for 10 min, the supernatant was subjected to further analyses.

2.10. Immunoblot analysis

SDS-PAGE was conducted using 4 μg each of recombinant *Eh*GGT-I, *Eh*FT, and recombinant rat GGT-I. Polyclonal antiserum against recombinant *Eh*GGT-I was commercially raised in a rabbit by Takara-Bio (Ohtsu, Japan) by four injections of 0.8 mg of the purified recombinant protein with Freund's complete and incomplete adjuvant at 2-week intervals. Two weeks after the last immunization, the immune serum was collected. Immunoblot analysis was performed as described [37] using primary antibodies at 1:100 and peroxidase-conjugated anti-rabbit IgG antibody (ICN-Cappel, Cappel, OH) at 1:1000. The blots were visualized with 4-chloro-1-naphthol and hydrogen peroxide.

2.11. Enzyme assays

The enzymatic activity of recombinant GGT-I and the whole lysate of *E. histolytica* trophozoites were assayed by measuring the incorporation of [^{3}H] GGPP or [^{3}H] FPP into the recombinant small GTPases of *E. histolytica*, human H-Ras-CVLL, or H-Ras-CVLS. The assay was performed essentially as described previously [38] with minor modifications. Briefly, in standard assays, the reaction mixture contained, in a total volume of 50 μl, 50 mM HEPES, pH 7.5, 5 mM $MgCl_2$, 25 μM $ZnCl_2$, 5 mM DTT, 0.1% PEG 20,000, 130 nM [^{3}H] GGPP (3 μCi/ml) or 187 nM [^{3}H] FPP (3 μCi/ml), 1.8 μg (1.8 μM) of the acceptor, and 2.4 μg (0.6 μM) of the purified recombinant GGT-I or 140 μg of the *E. histolytica* lysate. The reaction was initiated by the addition of either the recombinant enzyme or cell extracts, was run at 30 °C for 20 min, and terminated by the addition of 200 μl of 10% HCl in ethanol. The quenched reactions were allowed to stand at room temperature for 15 min. After the addition of 200 μl of 100% ethanol, the reactions were vacuum-filtered through a glass filter GF/C (Whatman, Maidstone, UK) using a Sampling Manifold (Millipore Corporation, Bedford, MA). The filters were washed with 4 ml of absolute ethanol, and then subjected to scintillation counting (LS 6000IC, Beckman Coulter, Fullerton, CA). The K_m values were calculated from Lineweaver–Burk plots. GGT-I assays were also conducted in the presence of known peptidomimetic inhibitors of GGT-I (GGTI-287 and GGTI-297) under the conditions described above.

3. Results

3.1. Features of GGT-Iβ from E. histolytica

A nucleotide sequence of *Eh*GGT-Iβ obtained by PCR was identical to the sequence available from the genome database (40.m00215). The predicted protein-coding region of *Eh*GGT-Iβ, consisting of 1014 bp, encodes a protein of 337 amino acids with a calculated molecular mass of 38.2 kDa and a p*I* of 6.71. A search for previously identified domains and motifs [39] using the NCBI Conserved Domain Search revealed that *Eh*GGT-Iβ possessed one CAL1 domain and two "prenyltransferase and squalene oxidase repeats" (Fig. 1). The deduced protein sequence of *Eh*GGT-Iβ was aligned with those of other organisms using the CLUSTAL W program (Fig. 1). *Eh*GGT-Iβ is the smallest in size, and apparently lacks the secretory signal sequence, organelle targeting signals, and domains implicated in membrane association including the transmembrane domain and myristoylation signal. *Eh*GGT-Iβ revealed a 22–30% positional identity with the GGT-Iβ of *Saccharomyces cerevisiae*, *Caenorhabditis elegans*, *Drosophila melanogaster*, *Homo sapiens*, or *Arabidopsis thaliana*. Among 12 residues implicated in making contact with peptide substrates in mammalian GGT-Iβ [40], four important residues Ala^{123}, Met^{124}, Arg^{202}, and Leu^{320} in *Hs*GGT-Iβ, were replaced by Ser^{107}, Tyr^{108}, Ser^{189}, and Met^{304}, respectively, in *Eh*GGT-Iβ, (Fig. 1). Furthermore, among 17 residues implicated in making contact with isoprenoid in mammalian GGT-Iβ [40], five residues, Phe^{52}, Thr^{127}, Cys^{177}, Phe^{324}, and Asn^{345} of *Hs*GGT-Iβ, were replaced by Met^{47}, Ala^{111}, Ser^{164}, Cys^{308}, and Il^{329}, respectively, in *Eh*GGT-Iβ (Fig. 1). All three residues implicated in the interaction with zinc in the catalytic center of mammalian GGT-Iβ [40] were conserved in *Eh*GGT-Iβ.

3.2. Phylogenetic analysis of EhGGT-Iβ and EhFTβ

A phylogenetic tree of GGT-Iβ and FTβ from *E. histolytica* and other organisms was constructed (Fig. 2). The β subunit of GGT-I and FT formed statistically significant (i.e. supported with 100% bootstrap proportion) well-separated clades, suggesting that the separation of GGT-I and FT occurred prior to the separation of these species. The β subunit of amebic GGT-I is divergent from those from all the other organisms including mammals; the overall shapes of these two trees are, however, significantly different. These results indicate that the catalytic β subunits of *Eh*FT and *Eh*GGT-I evolved independently to gain phylogenetic positions well separate from other eukaryotes, consistent with the presence of the unique biochemical properties of *Eh*GGT-I (see below).

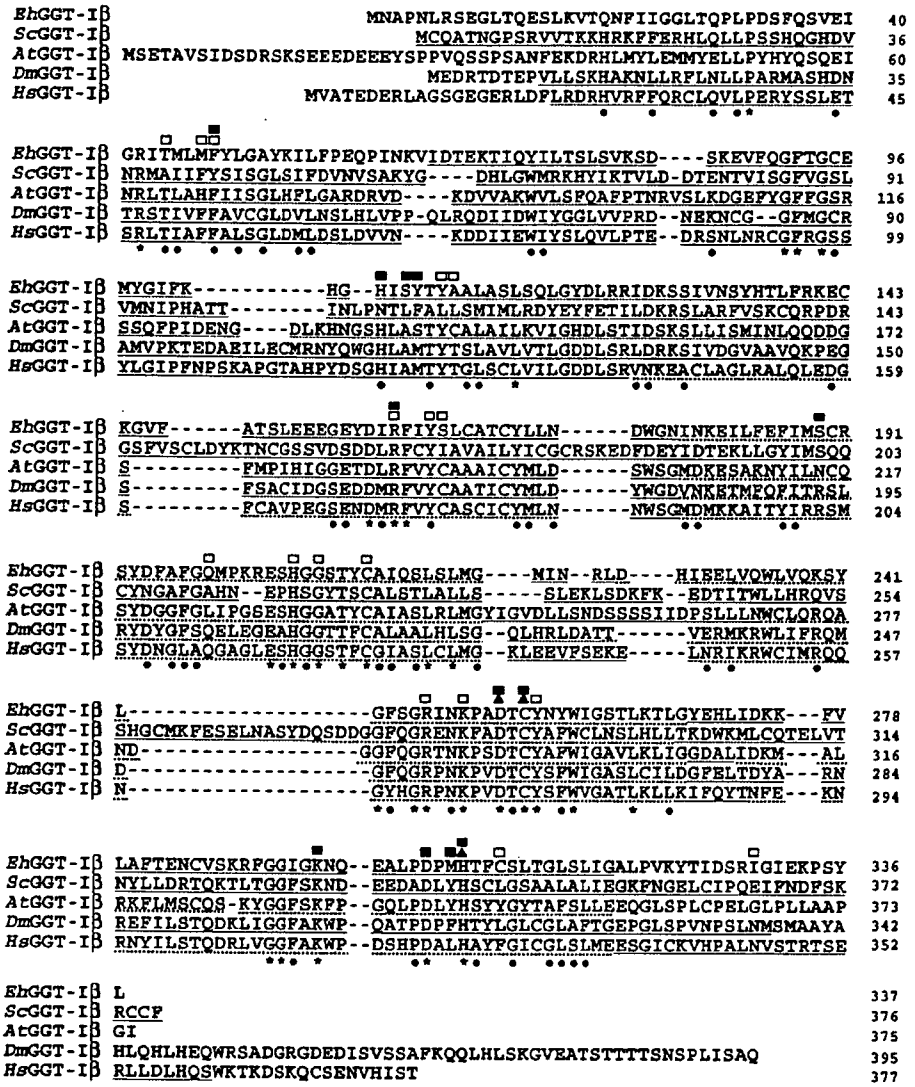

Fig. 1. Alignment of the deduced amino acid sequences of the β subunit of protein geranylgeranyltransferase I from *Entamoeba histolytica* and other organisms. *Eh, E. histolytica; Sc, Saccharomyces cerevisiae; At, Arabidopsis thaliana; Dm, Drosophila melanogaster; Hs, Homo sapiens*. The *asterisks* (*) under the alignments indicate identical amino acid residues and the *dots* (●) indicate conserved amino acid substitutions. CAL1 domains detected by the NCBI Conserved Domain Search are *underlined* (partially *dotted-underlined*). The prenyltransferase/squalene oxidase repeats, also detected by the search, are *dotted-underlined*. Amino acids implicated in the binding of isoprenoids or peptide substrates [40] are marked with *open* or *filled squares*, respectively. Amino acids implicated in the coordination of zinc are marked with *filled triangles*. DDBJ/EMBL/GeneBank™ accession numbers are given in Fig. 2.

3.3. Demonstration of GGT activity of the recombinant EhGGT-I against human Ras proteins

*Eh*GGT-Iα, identical to the previously characterized *Eh*FTα [26], and *Eh*GGT-Iβ were co-expressed in *E. coli*, and the complex was co-purified as described in Section 2. The purified complex revealed two major proteins of an equal intensity with an apparent molecular mass of 38 and 36 kDa on SDS-PAGE analysis (Fig. 3). Although the apparent molecular mass of the recombinant α subunit agreed well with the theoretical value of 37.6 kDa (of the native protein) with the amino- and carboxyl-terminal addition of Met-Arg-Gly-Ser-His-His-His-His-His-His-Thr-Asp-Pro and Gly-Gly-Phe, respectively, β subunit of 36 kDa was smaller than the theoretical value of 38.2 kDa for *Eh*GGT-Iβ. The molecular identity of these two subunits was confirmed using immunoblot analysis (see below). Densitometric quantitation of these two bands also supported the premise that they contain an equal number of protein molecules (data not shown). Thus, the recombinant *Eh*GGT-Iα and *Eh*GGT-Iβ were present as a stable complex with a stoichiometric ratio of 1:1 in the process of purification by Ni-nitrilotriacetic acid (NTA) agarose (Fig. 3). A rabbit antiserum raised against the recombinant *Eh*GGT-I reacted with both the α and β subunits of *Eh*GGT-I and the α subunit of *Eh*FT, but neither with the β subunit of *Eh*FT nor rat GGT-I (Fig. 3B and C). These data confirmed the identity of *Eh*GGT-Iα

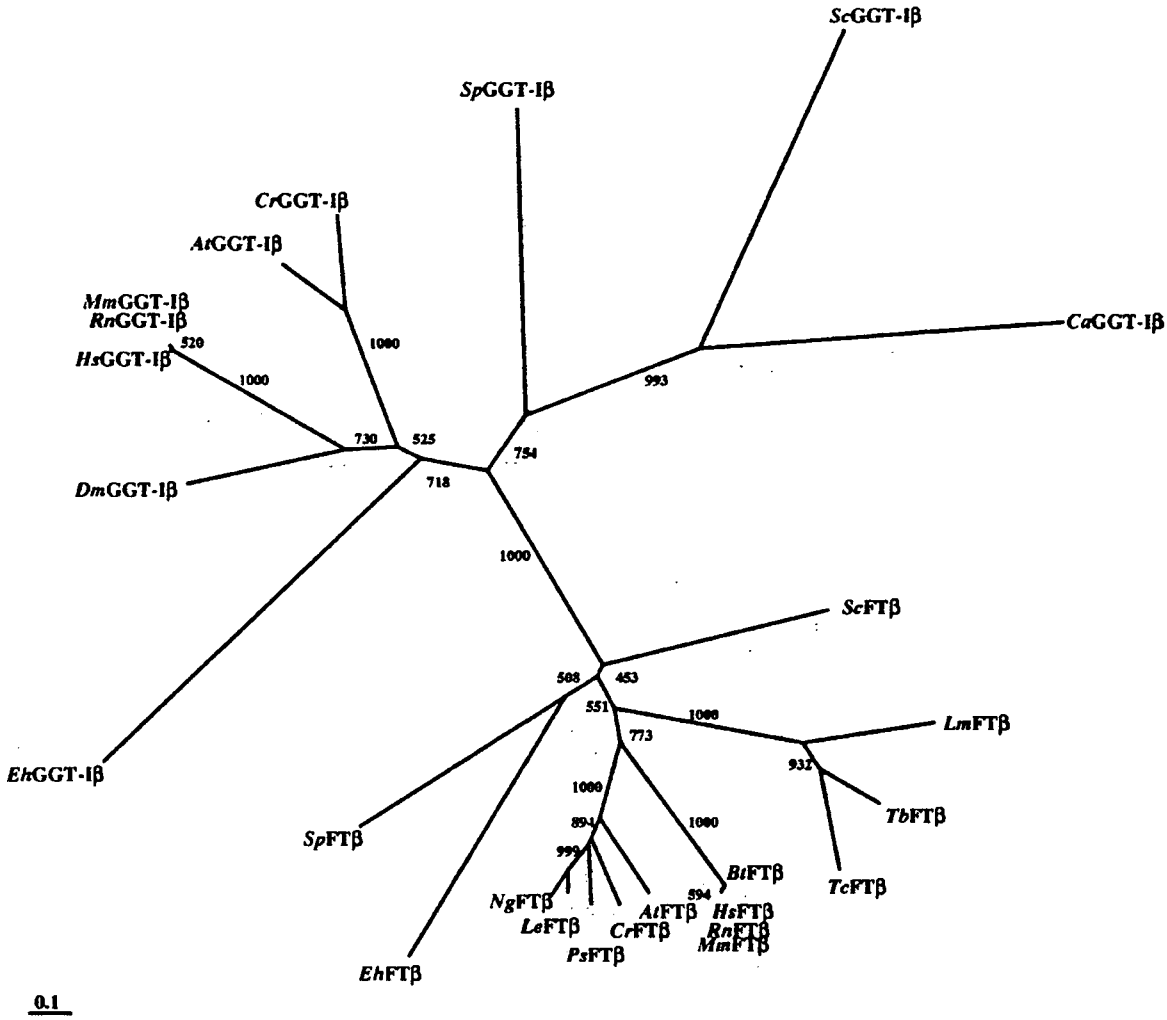

Fig. 2. Phylogenetic tree of the β subunits of GGT-I and FT. The tree was constructed by neighbor-joining distance analysis using the CLUSTAL W and TreeView programs. Line lengths indicate distances between nodes. The bar represents a distance of 0.1 amino acid change per site. Bootstrap values for 1000 replicates are shown at the nodes. Abbreviations are: *Eh*, *E. histolytica* (DDBJ/EMBL/GeneBank™ number of FTβ and GGT-Iβ, BAC98942, AB161971); *Sc*, *S. cerevisiae* (P22007, P18898); *Sp*, *Schizosaccharomyces pombe* (013782, P32434); *Tb*, *Trypanosoma brucei* (AAF73920, none); *Tc*, *T. cruzi* (AAL69905, none); *Lm*, *Leishmania major* (AAL69907, none); *At*, *A. thaliana* (AAF74564, NP_81487); *Ng*, *Nicotiana glutinosa* (AAB38796, none); *Ps*, *Pisum sativum* (Q04903, none); *Le*, *Lycopersicon esculentum* (AAC49666, none); *Cr*, *Catharanthus roseus* (AAQ02809, AAP50511); *Ca*, *Candida albicans* (none, AAD32539); *Dm*, *D. melanogaster* (none, AAC46972); *Mm*, *Mus musculus* (NP_666039, NP_766215) *Rn*, *Rattus norvegicus* (Q02293, P53610); *Bt*, *Bos taurus* (P49355, none); *Hs*, *H. sapiens* (NP_002019, NP_005014).

and *Eh*GGT-Iβ to the two corresponding bands on SDS-PAGE. They also suggest that antigenicity differed between the β subunits of *Eh*GGT-I and *Eh*FT and between *Eh*GGT-I and rat GGT-I.

Recombinant *Eh*GGT-I showed comparable GGT activity against both wild-type human recombinant H-Ras-CVLS [1.36 ± 0.028 (mean ± standard deviation of the mean) nmol GGPP/mg protein] and mutant H-Ras-CVLL (1.65 ± 0.013 nmol GGPP/mg protein), whereas rat GGT-I showed activity of a similar level against H-Ras-CVLL (1.83 ± 0.162), but no detectable activity against H-Ras-CVLS (Fig. 4), suggesting the presence of marked differences in acceptor specificity between *E. histolytica* and rat GGT-I.

3.4. Specificities of *Eh*GGT-I for acceptors and prenyl donors

We further examined the acceptor (i.e. protein substrate) specificity of *Eh*GGT-I toward amebic small GTPases, *Eh*Ras, *Eh*Rac, and *Eh*Rap. We tested if *Eh*GGT-I utilizes a limited range of substrates among possible small GTPases, as previously demonstrated for *Eh*FT, which showed very strict substrate specificity predominantly against *Eh*Ras4-CVVA [26]. The recombinant *Eh*GGT-I showed GGT activity toward all the tested *Eh*Ras proteins: *Eh*Ras1-CIMF, *Eh*Ras2-CELL, *Eh*Ras3-CSVM, and *Eh*Ras4-CVVA, with *Eh*Ras2 being the best substrate (Fig. 4). Notable differences in GGT-I activity exist depending upon the Ras species. For example, GGT-I activity

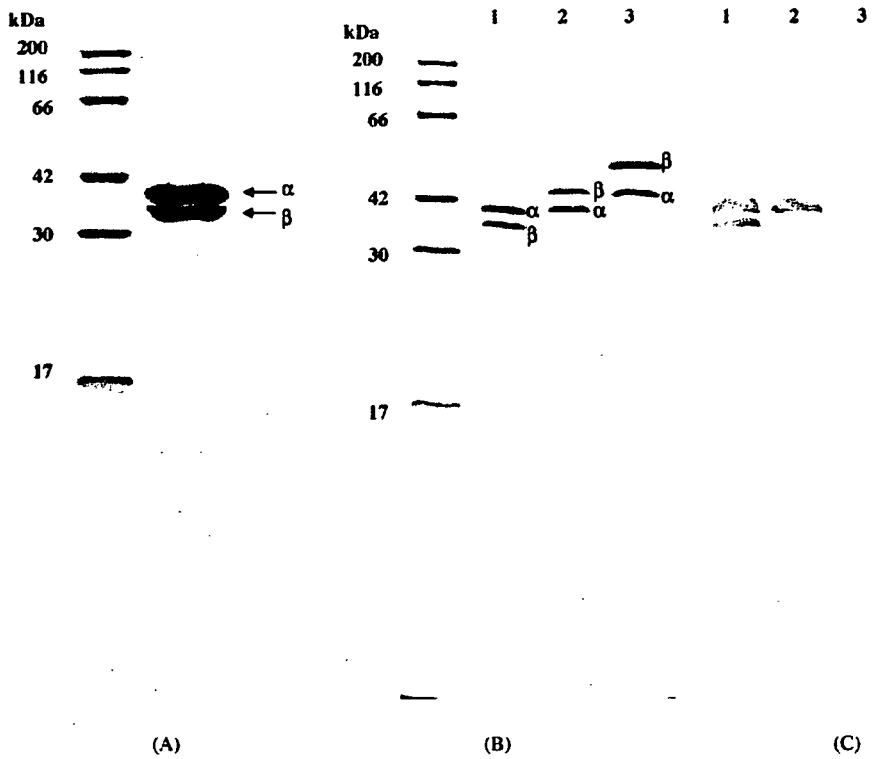

Fig. 3. SDS-PAGE and immunoblot analyses of the purified recombinant GGT-I of *E. histolytica*. (A) *Eh*GGT-1α and β subunits were coexpressed in *Escherichia coli* and purified on Ni-NTA agarose. The samples were subjected to SDS-PAGE and stained with Coomassie Brilliant Blue. (B) Approximately 4 μg each of recombinant *Eh*GGT-I (*Lane* 1), *Eh*FT (*Lane* 2) and rat GGT-I (*Lane* 3) were subjected to SDS-PAGE and stained with Coomassie Brilliant Blue. (C) The same samples in (B) were subjected to SDS-PAGE, transferred, and immunostained with rabbit antiserum against recombinant. *Eh*GGT-I.

toward *Eh*Ras2-CELL was >100 times higher than *Eh*Ras3-CSVM. The recombinant *Eh*GGT-I also transferred geranylgeranyl to *Eh*RacA-CLLF, *Eh*RacC-CALL, *Eh*RacG-CSLF, *Eh*Rapl-CSLL, and *Eh*Rap2-CSLF (Fig. 4). In contrast, rat GGT-I revealed comparable activity against *Eh*RacA-CLLF, *Eh*RacG-CSLF; however, rat GGT-I showed almost no detectable activity against the other three *Eh*Ras proteins and significantly lower activity against *Eh*RacC-CALL, *Eh*Rapl-CSLL, and *Eh*Rap2-CSLF. We also assayed for GGT activity in the whole lysate of the *E. histolytica* trophozoites. GGT activity (4.9–9.4 pmol GGPP/mg protein) was detected against *Eh*Ras 1-4 and human H-Ras-CVLL in the whole lysate, verifying the presence of GGT activity against these representative Ras proteins (data not shown).

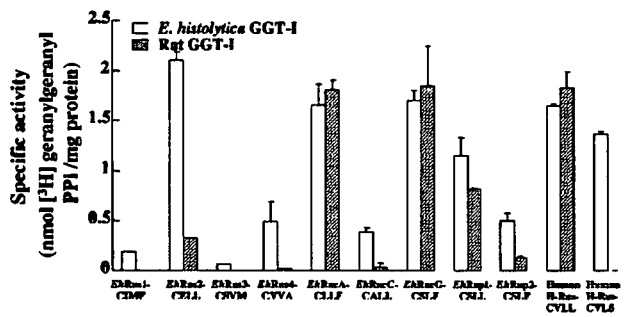

Fig. 4. Protein substrate specificity of recombinant GGT-I of *E. histolytica*. The specific activity of the recombinant *Eh*GGT-I was determined by the incorporation of [^{3}H] geranylgeranyl pyrophosphate into the recombinant *Eh*Ras1-4, *Eh*Rac A, C, G, *Eh*Rapl, 2, wild-type H-Ras-CVLS, and mutant H-Ras-CVLL. The reaction mixture (50 μl) contained 50 mM HEPES, pH 7.5, 5 mM $MgCl_2$, 25 μM $ZnCl_2$, 5 mM DTT, 0.1% PEG 20,000, 130 nM [^{3}H] GGPP (3 μCi/ml), 1.8 μg (1.8 μM) of an acceptor, and 2.4 μg (0.6 μM) of the purified recombinant GGT-I. Means ± standard errors of quadruplicates are shown. DDBJ/EMBL/GeneBank™ accession numbers of these proteins are: *Eh*Rasl, AAA21446; *Eh*Ras2, AAA21447; *Eh*Ras3, BAD07406; *Eh*Ras4, BAB07407; *Eh*RacA, Q24814; *Eh*RacC, Q24816; *Eh*RacG, O76321; *Eh*Rapl, AAA21444; *Eh*Rap2, AAA21445; H-Ras-CVLS, P01112.

We examined the specificity of the prenyl donors of *Eh*GGT-I and rat GGT-I. The recombinant *Eh*GGT-I showed farnesyl transferase activity against *Eh*Ras2-CELL and H-Ras-CVLL at about 27% the efficiency of geranylgeranyltransferase. In contrast, rat GGT-I showed significantly lower FT activity against the same acceptors (3.3–6.6% of GGT-I activity) (data not shown).

3.5. Kinetic properties of EhGGT-I

Lineweaver-Burk plots showed the K_m of recombinant *Eh*GGT-I for *Eh*Ras2 and H-Ras-CVLL to be 0.85 ± 0.11 and 0.2 ± 0.01 μM (plots not shown), respectively. The K_m of recombinant rat GGT-I for H-Ras-CVLL was 6 times higher (1.2 μM [41]), suggesting the higher substrate affinity of the amebic GGT-I toward protein acceptors. *Eh*GGT-I showed a K_m of 0.20 ± 0.05 μM for GGPP (using H-Ras-CVLL as a protein substrate), which is four times lower than that of rat GGT-I

Table 1
Inhibition of recombinant GGT-I from *Entamoeba histolytica* and rat by peptidomimetics

Inhibitors	IC_{50} (μM)			
	E. histolytica GGT-I		Rat GGT-I	
	*Eh*Ras2-CELL	H-Ras-CVLL	*Eh*Ras2-CELL	H-Ras-CVLL
GGTI-287	5.5 ± 1.8	25.3 ± 7.6	0.063 ± 0.004	0.049 ± 0.02
GGTI-297	3.2 ± 0.4	2.1 ± 0.3	0.033 ± 0.004	0.257 ± 0.03

The reaction mixture contained, in a total volume of 50 μl, 50 mM HEPES, pH 7.5, 5 mM $MgCl_2$, 25 μM $ZnCl_2$, 5 mM DTT, 0.1% PEG 20,000, 130 nM [^{3}H] GGPP (3 μCi/ml), 1.8 μg (1.8 μM) of the acceptor, and 2.4 μg (0.6 μM) of the recombinant GGT-I. IC_{50} of each peptidomimetics was determined by measuring specific activities with a range of 0.01–100 μM of the compounds.

(0.81 ± 0.27 μM). *Eh*GGT-I also showed a higher affinity for FPP than rat GGT-I; the K_m of *Eh*GGT-I or rat GGT-I for FPP using H-Ras-CVLL was 29.8 ± 3.7 or >400 nM, respectively.

3.6. Sensitivity of recombinant EhGGT-I to inhibitors of mammalian GGT-I

We examined the sensitivity of *Eh*GGT-I to known peptidomimetic GGT-I inhibitors. As shown in Table 1, *Eh*GGT-I was eight and 516 times more resistant to GGTI-287 than rat GGT-I when recombinant *Eh*Ras2-CELL and H-Ras-CVLL were used as substrates, respectively. *Eh*GGT-I was also 97 and eight times less sensitive to GGTI-297 than rat GGT-I, respectively.

4. Discussion

In this study, we demonstrated marked biochemical differences in the major prenyl enzyme responsible for the lipid modification of Ras and Rho/Rac small GTPases between the enteric protozoan parasite and its mammalian host. This study represents the first biochemical characterization of GGT-I from unicellular protozoa. Our genome-wide search of a GGT-Iβ gene among parasitic protozoa, together with the previous report on the lack of GGT-I activity in kinetoplastids [9], indicates that all protozoan parasites except for *E. histolytica* where the genome database is available lack GGT-I, reinforcing the peculiarity of *E. histolytica*, which possesses both FT and GGT-I. This apparent redundancy of the isoprenylation pathways may be associated with unique features of functions and regulations of Ras/Rap and Rho/Rac proteins through unusual lipid modifications in this parasite. It is totally unknown why *E. histolytica* mainly utilizes GGT-I for lipid modification of a majority of Ras/Rap and Rho/Rac and employs FT for isoprenylation of a very limited subset of Ras isotypes (solely *Eh*Ras4), while the other parasitic protists possess only FT and are likely to have lost GGT-I during parasitic or non-parasitic evolution.

Phylogenetic analyses indicate that *Eh*GGT-Iβ, as well as *Eh*GGT-Iα (*Eh*FTα) in our previous study [26], is only distantly associated with homologues from other organisms. This may partially explain why the unique biochemical properties of the amebic GGT-I that are not shared by its mammalian counterpart exist (see below). Our previous study suggested that α and β subunits of FT co-evolved at a comparable rate among organisms because the phylogenetic trees of the two FT subunits were almost identical [26]. However, the phylogenetic relationship of the β subunit of GGT-I is apparently distinct from that of α and β subunits of FT, refuting a hypothesis of the co-evolution of these two isoprenylation enzymes (Fig. 2).

The results of the GTPase substrate specificity of *Eh*GGT-I indicate that the Ras, Rac, and Rap proteins possessing CaaL, CaaF, CaaM, CaaA, or CaaS at the carboxyl terminus, either from *E. histolytica* or humans, can serve as acceptors for *Eh*GGT-I. Thus, the amebic GGT-I utilizes a broad range of small GTPases for geranylgeranylation. This is in striking contrast to the farnesylation of small GTPases by *Eh*FT, which showed an extremely limited substrate range; only *Eh*Ras4 can serve as a farnesyl acceptor. Our database analysis showed that *E. histolytica* Ras/Rap, Rho/Rac, and Rab with the CaaX terminus possess terminal Leu (42%), Phe (32%), Val (13%), Cys/Met (4% each), or Ala/Ser/Ile (2% each) (data not shown). In mammals, small GTPases with Leu and Val are exclusively geranylgeranylated by GGT-I, and those with Met, Gln, Ser, Ala, Thr, or Cys (in the order of frequency) are solely farnesylated by FT, while those with Phe are modified by both enzymes [42]. In contrast to the amebic GGT-I, mammalian GGT-I does not geranylgeranylate small GTPases with terminals Ala and Ser. Thus, the unique geranylgeranlylation of these small GTPases possessing terminal Ala or Ser in the ameba may confer a unique role to these GTPases. *E. histolytica* small GTPases with the CaaX terminus shows deviation toward Phe at the X position as shown above. However, amebic FT cannot utilize small GTPases terminating with Phe [26]. Taken together, this enteric protozoon strongly relies on GGT-I. It is conceivable that there are biological selections toward the current predominant utilization of GGT-I in this organism. For instance, since the farnesylation of CENP-E, a centromere-associated protein playing a critical role in cell cycle progression in mammals [43], is not present in *E. histolytica*, its modifying enzyme is not required because the isoprenylation of most of small GTPases, except for *Eh*Ras4, is accomplished by GGT-I and GGT-II (Rab GGT, Kumagai, M., Makioka, A., Takeuchi, T. and Nozaki, T., unpublished).

A comparison of ternary complexes of mammalian GGT-I and FT revealed that acceptor specificity is partially determined by surface complementarity between the X residue and the "specificity pocket," to which the side chain of the X residue binds [40]. For instance, the hydrophobic "specificity pocket" discriminates against polar side chains. In addition, the shape and volume of the "specificity pocket" further restrict the range of amino acids most preferably to Leu for GGT-I [40]. However, this preference for Leu was not observed for *Eh*GGT-I. It is intriguing that while the amebic GGT-I prefers *Eh*Ras2-CELL to the other three isotypes of *Eh*Ras possessing Phe, Met, or Ala at the carboxyl terminus (4–33 times in specific activity), it showed an opposite preference for Rac with carboxyl-terminal Phe (*Eh*RacA and *Eh*RacG) over Leu (*Eh*RacC). This observed discrepancy on the acceptor preference of the amebic GGT-I is not artifactual since FT revealed a reverse preference (i.e. approximately eight times higher activity against *Eh*Ras1 than

*Eh*Ras2; [26]). These data suggest that the acceptor specificity of the amebic GGT-I is strongly influenced by neighboring residues of GGT-I other than the carboxyl terminus or tertial structure of small GTPases, which is remarkably different from mammalian GGT-I [42]. The data also indicate that the interaction between the surface of GGT-I and the upstream hyper variable region of small GTPases may differ between ameba and mammals. Although the carboxyl terminus of both *Eh*Rasl and *Eh*Ras2 is highly charged (the 17-a.a. carboxyl-terminal region contain nine or seven positively-charged and three or two negatively-charged amino acids in *Eh*Rasl or *Eh*Ras2, respectively), the total polarity of the carboxyl terminus of *Eh*Rasl is significantly higher than *Eh*Ras2. These changes may produce steric differences that lead to changes in substrate specificity. Note that the four substitutions among 12 residues implicated to bind a peptide substrate in mammalian GGT-Iβ [40] (Ala^{123} to Ser^{107}, Met^{124} to Tyr^{108}, Arg^{202} to Ser^{189}, and Leu^{320} to Met^{304}) in *Eh*GGT-Iβ result in the emergence of two hydroxyl-containing residues and the loss of one positive amino acid. The tertial structure of mammalian GGT-I revealed that Ala^{123} and Met^{124} in mammalian GGT-I do not directly interact with X residue of the protein substrate [42], but position close to the X residue. It is conceivable that substituting these amino acids with hydroxyl-containing Ser and aromatic Tyr, respectively, significantly influences the shape and charge of the end of the protein substrate-binding pocket, which likely results in the wider specificity of the amebic GGT-I for protein substrates.

*Eh*GGT-I also utilizes a wider range of isoprenyl donors. *Eh*GGT-I showed four to nine times higher farnesyltransferase activity than rat GGT-I. Five out of 17 residues implicated in the binding of isoprenoid in mammalian GGT-Iβ [40] are substituted in *Eh*GGT-Iβ (Fig. 1). Among these five substitutions (Phe^{52} to Met^{47}, Thr^{127} to Ala^{111}, Cys^{177} to Ser^{164}, Phe^{324} to Cys^{308}, and Asn^{345} to Ile^{329}) in *Eh*GGT-Iβ, Phe^{324} to Cys^{308} is worth noting. Phe^{324} of rat GGT-Iβ is in close proximity to the end of the C20 geranylgeranyl chain and is partially responsible, together with Thr^{49} (also conserved in *Eh*GGT-Iβ), for allowing rat GGT-I to accommodate GGPP in the catalytic pocket [40]. It is conceivable that Phe^{324} to Cys^{308} substitution creates additional water-mediated or non-mediated hydrogen bonds with neighboring residues, which result in the ability of *Eh*GGT-Iβ to utilize FPP as well as GGPP. This substitution may also influence the stability of the enzyme-product complex and the binding of fresh isoprenoid diphosphate to displace the prenyl-peptide product from the active site during the reaction cycle, as shown for rat GGT-I [40].

The amebic GGT-I revealed notable resistance to peptidomimetics known to inhibit mammalian GGT-I (Table 1). This apparent insensitivity of the amebic GGT-I to the inhibitors is not due to the impurity of our preparations since mixing our recombinant GGT-I with rat GGT-I did not influence the inhibition of rat GGT-I by these peptidemimetics. In addition, both amebic and rat GGT-I revealed comparable sensitivity against a GGPP derivative, 3-aza-2,3-dihydro-la-homo-GGPP (kindly donated by Prof. R.M. Coates, University of Illinois) (IC_{50}, approximately 4–10 μM), confirming the observed insensitivity of *Eh*GGT-I against GGTI-287 and GGTI-297. GGTI-287 and GGTI-297 are CaaL peptidomimetics, where reduced C is linked to Leu by 2-phenyl-4-aminobenzoic acid or by 2-naphthyl-4-aminobenzoic acid [44–46]. It is puzzling why the amebic GGT-I is insensitive to these CaaL peptidomimetics because *Eh*GGT-I shows wide donor specificity as discussed above.

Together with our previous study [26], this study indicates that most small GTPases with the CaaX motif from *E. histolytica* are geranylgeranylated or farnesylated by GGT-I, but not farnesylated by FT, which significantly differs from mammals where Ras and Rho/Rac proteins with CaaX are either farnesylated by FT or geranylgeranylated by GGT-I at a comparable frequency [42]. Thus, GGT-I is biologically and physiologically very important for *E. histolytica*, making *Eh*GGT-I an attractive, rational target for the development of new chemotherapeutics against amebiasis.

Acknowledgements

The authors thank Naohiro Watanabe, Jikei, for his valuable discussion and Yumiko Saito-Nakano, NIID, for immunoblotting and her helpful discussion. We also thank Tomomi Yamashita, Jikei, for her technical assistance. This work was supported by a Grant for Precursory Research for Embryonic Science and Technology (PRESTO), Japan Science and Technology Agency to T.N., a Health Sciences Research Grant for Research on Emerging and Re-emerging Infectious Diseases from the Ministry of Health, Labor, and Welfare to A.M. and T.N., Grant-in-Aid for Scientific Research from the Ministry of Education, Culture, Sports, Science and Technology of Japan to A.M. (13670256) and T.N. (16044250, 16017307, 15590378), and a Grant for the Project to Promote Development of Anti-AIDS Pharmaceuticals from the Japan Health Sciences Foundation to T.N. The database search was conducted with the 9× *E. histolytica* genome database available at the Institute for Genomic Research (TIGR) and the Sanger Institute with financial support from the National Institute of Allergy and Infectious Diseases and The Wellcome Trust.

References

[1] Zhang FL, Casey PJ. Protein prenylation: molecular mechanisms and functional consequences. Annu Rev Biochem 1996;65:241–69.
[2] Takai Y, Kaibuchi K, Kikuchi A, Kawata M. Small GTP-binding proteins. Int Rev Cytol 1992;133:187–230.
[3] Boguski MS, McCormick F. Proteins regulating Ras and its relatives. Nature 1993;366:643–54.
[4] Casey PJ, Seabra MC. Protein prenyltransferases. J Biol Chem 1996;271:5289–92.
[5] Maurer-Stroh S, Washietl S, Eisenhaber F. Protein prenyltransferases. Genome Biol 2003;4(212):1–9.
[6] James GL, Goldstein JL, Brown MS. Polylysine and CVIM sequences of K-RasB dictate specificity of prenylation and confer resistance to benzodiazepine peptidomimetic in vitro. J Biol Chem 1995;270:6221–6.
[7] Cox A, Der CJ. Farnesyltransferase inhibitors and cancer treatment: targeting simply Ras? Biochem Biophys Acta 1997;1333:F51–71.
[8] Gibbs JB. Ras C-terminal processing enzymes-new drug targets? Cell 1991;65:1–4.
[9] Gelb MH, Van Voorhis WC, Buckner FS, et al. Protein farnesyl and *N*-myristoyl transferases: piggy-back medical chemistry targets for the